

DEVELOPMENT OF THE MESOPUFF II DISPERSION MODEL

by

Joseph S. Scire

Frederick W. Lurmann

Arthur Bass

Steven R. Hanna

Environmental Research & Technology, Inc.

Concord, Massachusetts 01742

Contract No. 68-02-3733

Project Officer

James M. Godowitch

Meteorology and Assessment Division

Environmental Sciences Research Laboratory

Research Triangle Park, NC 27711

ENVIRONMENTAL SCIENCES RESEARCH LABORATORY

OFFICE OF RESEARCH AND DEVELOPMENT

U.S. ENVIRONMENTAL PROTECTION AGENCY

RESEARCH TRIANGLE PARK, NC 27711

**DEVELOPMENT OF THE MESOPUFF II DISPERSION MODEL**

**by**

**Joseph S. Scire**

**Frederick W. Lurmann**

**Arthur Bass**

**Steven R. Hanna**

**Environmental Research & Technology, Inc.**

**Concord, Massachusetts 01742**

**Contract No. 68-02-3733**

**Project Officer**

**James M. Godowitch**

**Meteorology and Assessment Division**

**Environmental Sciences Research Laboratory**

**Research Triangle Park, NC 27711**

**ENVIRONMENTAL SCIENCES RESEARCH LABORATORY**

**OFFICE OF RESEARCH AND DEVELOPMENT**

**U.S. ENVIRONMENTAL PROTECTION AGENCY**

**RESEARCH TRIANGLE PARK, NC 27711**

## DISCLAIMER

This report has been reviewed by the Environmental Sciences Research Laboratory, U.S. Environmental Protection Agency, and approved for publication. Approval does not signify that the contents necessarily reflects the views and policies of the U.S. Environmental Protection Agency, nor does mention of trade names or commercial products constitute endorsement or recommendation for use.

## PREFACE

This publication contains a technical description of the MESOPUFF II model and its processor programs. The preprocessor programs require hourly meteorological surface, twice-daily upper air, and hourly precipitation (optional) data in the formats archived by the National Climatic Center in Asheville, North Carolina. The model utilizes the Gaussian puff superposition approach to simulate a continuous pollutant plume. The model is capable of multi-day simulations and has algorithms for plume rise, transport, chemical transformations, dry deposition, and wet removal. Terrain variations are not accounted for in the model.

The puff superposition approach has not been used extensively in air quality models for the prediction of pollutant concentrations. MESOPUFF II is being made available to promote testing and evaluation of the methods and optional features in the model. MESOPUFF II has no regulatory standing and its application for regulatory purposes should be considered in light of EPA's Guideline on Air Quality Models.

The model version (1.0) documented in this publication represents an attempt to utilize recent scientific information to realistically account for the relevant physical processes active on the regional to long-range scales. Modifications may be made in the future based on results by users and findings from ongoing research programs.

Although attempts have been made to check the computer program code, errors may be found occasionally. Adjustments to the code to suit different computer systems may be required. If there is a need to correct, revise, or update this model, changes may be obtained as they are issued by completing and sending the form on the last page of the user guide.

It is anticipated that MESOPUFF II will be made available in the future on the User's Network for Applied Modeling of Air Pollution (UNAMAP) system. A tape of this model or the UNAMAP system may be purchased from NTIS for use on the user's computer system. For information on UNAMAP contact: Chief, Environmental Operations Branch, MD-80, U.S. Environmental Protection Agency, Research Triangle Park, NC 27711.

## ABSTRACT

The development of the MESOPUFF II regional-scale air quality model is described. MESOPUFF II is a Lagrangian variable-trajectory puff superposition model suitable for modeling the transport, diffusion and removal of air pollutants from multiple point and area sources at transport distances beyond the range of conventional straight-line Gaussian plume models (i.e., beyond  $\sim 10$ -50 km). It is an extensively modified version of the MESOScale PUFF (MESOPUFF) model (Benkley and Bass 1979). Major additions and enhancements include: use of hourly surface meteorological data and twice-daily rawinsonde data; separate wind fields to represent flow within and above the boundary layer; parameterization of vertical dispersion in terms of micrometeorological turbulence variables; parameterization of  $\text{SO}_2$  to  $\text{SO}_4^=$  and  $\text{NO}_x$  to  $\text{NO}_3^-$  conversion, including the chemical equilibrium of the  $\text{HNO}_3/\text{NH}_3/\text{NH}_4\text{NO}_3$  system; resistance modeling of dry deposition, including options for source or surface depletion; time- and space-varying wet removal; and a computationally efficient puff sampling function. The scientific and operational bases for these developments are described. The results of a preliminary evaluation of several model algorithms during a two-day period of the Tennessee Plume Study are also presented.

This report was submitted in fulfillment of Contract No. 68-02-3733 by Environmental Research & Technology, Inc. under sponsorship of the U.S. Environmental Protection Agency. This report covers the period from February 11, 1982 to March 15, 1983, and work was completed as of September, 1983.

## CONTENTS

Preface . . . . .	iii
Abstract . . . . .	iv
Figures . . . . .	vi
Tables . . . . .	vii
Acknowledgements . . . . .	viii
 1. Introduction . . . . .	 1
1.1 Background . . . . .	1
1.2 MESOPUFF II Modeling Package . . . . .	2
1.3 Major Features of MESOPUFF II . . . . .	4
1.4 Tennessee Plume Study . . . . .	8
2. Technical Developments . . . . .	10
2.1 Wind Field . . . . .	10
2.2 Micrometeorological Parameters . . . . .	14
2.3 Dry Deposition - Three Layer Model . . . . .	21
2.4 Chemical Transformations . . . . .	33
2.5 Wet Removal . . . . .	50
2.6 Puff Sampling Function . . . . .	55
3. Demonstration Model Run . . . . .	62
References . . . . .	72
Appendices	
A. Reactions and rate constants of the Atkinson et al. (1982) chemical mechanism . . . . .	77

## FIGURES

<u>Number</u>		<u>Page</u>
1	MESOPUFF II Modeling Package . . . . .	3
2	Schematic Representation of Puff Superposition Approach . . . . .	5
3	Particle Deposition to Water Surfaces . . . . .	24
4	SO <sub>2</sub> Deposition Velocities . . . . .	25
5	Comparison of Source Depletion and Surface Depletion Models . . . . .	31
6	Optional Three Layer System Used in MESOPUFF II. . .	32
7	SO <sub>2</sub> Oxidation Pathways . . . . .	35
8	NO <sub>x</sub> Oxidation Pathways . . . . .	36
9	NH <sub>4</sub> NO <sub>3</sub> Dissociation Constant Temperature and Relative Humidity Dependence . . . . .	39
10	Comparison of SO <sub>2</sub> Oxidation Rates Predicted by the ERT and Gillani et al. Equations . . . . .	47
11	Average Plume Sulfur Conversion Rate as a Function of Mean Time of Day of Plume Transport . . . . .	48
12	Washout Ratio as a Function of Precipitation Rate for Different Storm Types . . . . .	51
13	SO <sub>2</sub> Washout Ratio as a Function of pH and Temperature for Equilibrium Scavenging Conditions . . . . .	53
14	Location of Cumberland Steam Plant, Surface Meteorological Stations and Upper Air Rawinsonde Stations on Meteorological Grid. . . . .	64
15	Boundary Layer Growth and Plume Fumigation . . . . .	67
16	Observed and Predicted Mixing Heights in the Vicinity of the Cumberland Steam Plant . . . . .	68

## TABLES

<u>Number</u>		<u>Page</u>
1	Major Features of MESOPUFF II . . . . .	7
2	Options for Lower and Upper Wind Fields . . . . .	12
3	Solar Radiation Reduction Factor $\beta$ . . . . .	17
4	Factors Influencing Dry Deposition Removal Rates. .	22
5	Summertime SO <sub>2</sub> Canopy Resistances as a Function of Land Use Type and Stability Class . .	28
6	Parameter Variations in the Photochemical Modeling Simulations . . . . .	43
7	Default Values of the Scavenging Coefficient, $\lambda$ (s <sup>-1</sup> ) . . . . .	54
8	Conversion of Reported Precipitation Type/ Intensity to Precipitation Codes . . . . .	56
9	Effect of Sampling Rate, N, on Predicted Near- Field Concentrations for Two Sampling Algorithms. .	60
10	Model Run Parameters Used in Demonstration Run. . .	65
11	History of Puff Released 8/23/78 Hour 1 . . . . .	66
12	Observed and Predicted SO <sub>2</sub> Conversion Rates . . . .	70

## ACKNOWLEDGEMENTS

The authors wish to acknowledge the contributions made by Drs. A. Venkatram and R. Yamartino to the development of MESOPUFF II. The assistance and advice of the EPA project officer, James Godowitch, is appreciated.

## SECTION 1

### INTRODUCTION

#### 1.1 Background

The regional and long-range transport and transformation of sulfur oxides and nitrogen oxides emitted from major point sources are of increasing concern. Motivated by the need for easily-used, cost-efficient mesoscale air quality models suitable for regulatory applications, the National Oceanic and Atmospheric Administration (NOAA) sponsored a study by Environmental Research & Technology, Inc. (ERT) to develop, compare, and evaluate a set of mesoscale models and related processor programs known as the MESO-models (Benkley and Bass 1979a, b, c; Morris et al. 1979; Scire et al. 1979). One of these models, the MESOscale PUFF (MESOPUFF) model appears to be well suited for regulatory use. For this reason, the Environmental Protection Agency (EPA) has sponsored a second study by ERT to enhance the capabilities and flexibility of the MESOPUFF model to meet the current and future needs of EPA in predicting mesoscale transport of pollutants, especially secondary aerosols.

This report is the first volume of a two-volume set describing the results of this effort to extent MESOPUFF's capabilities. Extensive modifications have been made to MESOPUFF in order to refine and enhance its treatment of advection, vertical dispersion, removal and transformation processes. The new model has been designated MESOPUFF II. The objective of this document is to describe the scientific and operational bases for the most significant modifications made to MESOPUFF. In addition, this document provides the results of a demonstration run of the model for a two-day period during the Tennessee Plume Study (TPS). The companion report, entitled "User's Guide to the MESOPUFF II Model and Related Processor Programs" provides a summary of the basic model equations and includes a

complete set of user instructions for the MESOPUFF II model and its processor programs (READ56, MESOPAC II, MESOFILE II). The User's Guide also contains a description of several model algorithms not presented in this document that were unchanged or only slightly modified (e.g., the puff trajectory function, dispersion coefficient calculations and the plume rise algorithm).

In the next section, the MESOPUFF II modeling package is outlined and the functions of each program are discussed. Section 1.3 contains a summary of the major modifications made in MESOPUFF II. The TPS is briefly described in Section 1.4. The second chapter contains a technical description of model algorithms. A description of a demonstration run of the model for two days during the TPS and the results are contained in the third chapter.

## 1.2 MESOPUFF II Modeling Package

The MESOPUFF II model is one element of an integrated modeling package. This modeling package (Figure 1) also contains components for preprocessing of meteorological data (READ56, MESOPAC II) and postprocessing of predicted concentration results (MESOFILE II). Each component of the MESOPUFF II modeling package is briefly described below.

READ56 is a preprocessor program that reads and processes the twice-daily upper air wind and temperature sounding data available from the National Climatic Center (NCC) for selected stations. READ56 extracts the data required by the MESOPAC II program from a standard-formatted NCC tape (TDF5600). READ56 scans the upper air data for completeness; warning messages are printed to flag missing or incomplete soundings. A file of processed sounding data is created in a format convenient for possible editing by the user and it is subsequently input into the MESOPAC II program.

MESOPAC II is the meteorological processor program that computes the time and space interpolated fields of meteorological variables (e.g., transport winds, mixing height) required by MESOPUFF II to describe

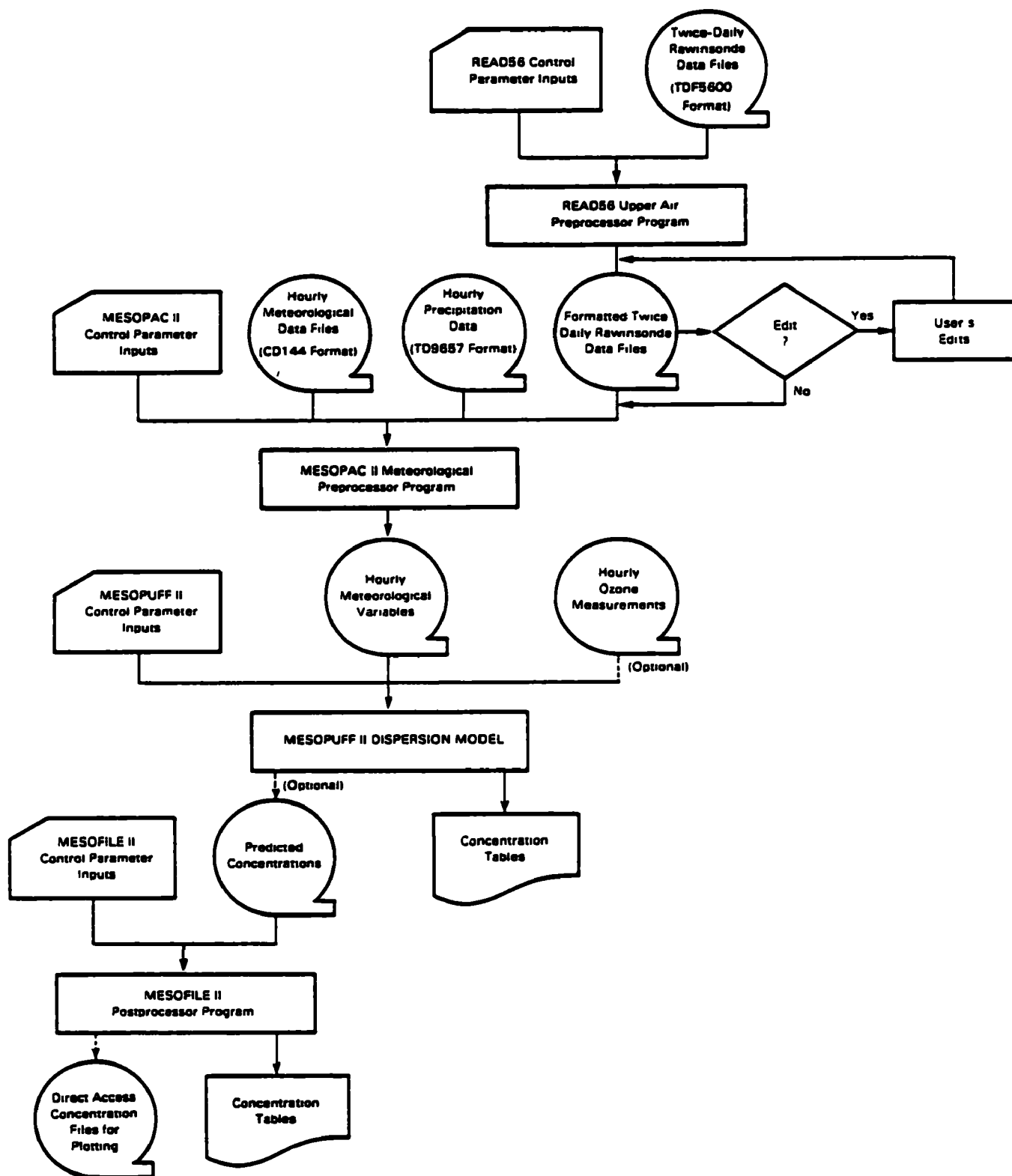


Figure 1 MESOPUFF II Modeling Package

mesoscale transport and dispersion processes. MESOPAC II reads the upper air data files created by READ56 and files of standard-formatted NCC hourly surface meteorological data (CD144) and hourly precipitation data (TD9657). A single output file containing observed and derived meteorological fields is produced which serves as an input file to MESOPUFF II.

MESOPUFF II is a Gaussian, variable-trajectory, puff superposition model designed to account for the spatial and temporal variations in transport, diffusion, chemical transformation and removal mechanisms encountered on regional scales. With the puff superposition approach, a continuous plume is modeled as a series of discrete puffs (Figure 2). Each puff is transported independently of other puffs. A puff is subject to growth by diffusion, chemical transformations, wet removal by precipitation, and dry deposition at the surface. Up to five pollutants may be modeled simultaneously.

MESOFIELD II is a postprocessing program that operates on the concentration file produced by MESOPUFF II. The postprocessing functions available with MESOFIELD II include flexible time averaging of gridded or non-gridded (discrete) receptor concentrations, line printer contour plots of concentration fields, statistical analysis of point-by-point or bulk differences between concentration fields, and summing and scaling capabilities.

### 1.3 Major Features of MESOPUFF II

The original MESOPUFF model is a single-layer, two species puff superposition model. Its meteorological preprocessor (MESOPAC) creates gridded fields of wind components, mixing height, and stability class from twice-daily rawinsonde (upper air) data. Chemical transformation of sulfur dioxide to sulfate is modeled with a spatially and temporally constant transformation rate. Dry deposition is modeled with a constant deposition velocity for each pollutant by the source depletion technique.

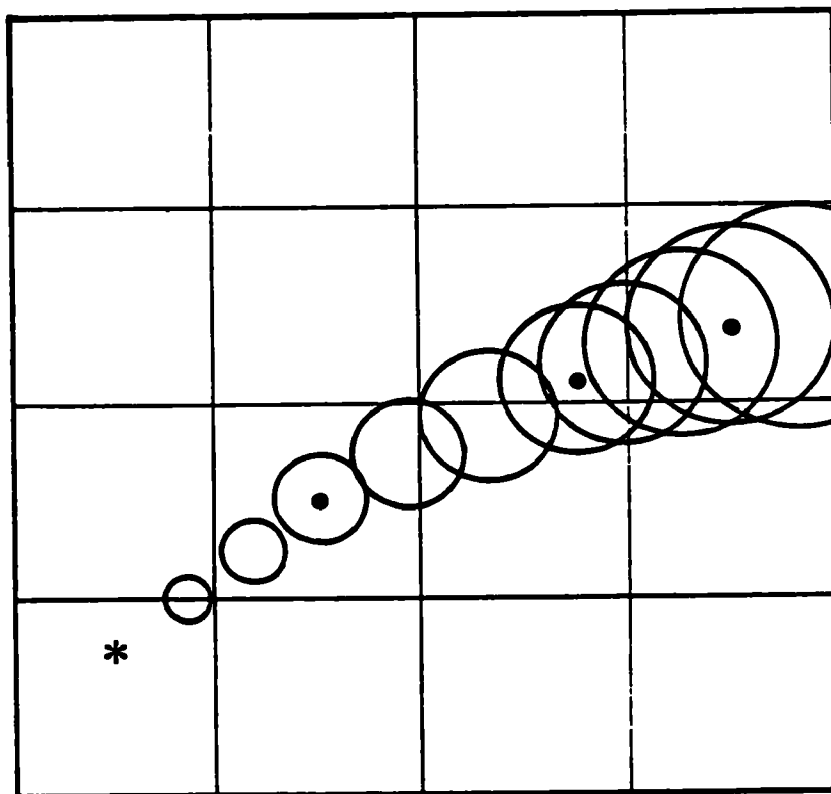


Figure 2 Schematic Representation of Puff Superposition Approach

Table 1 outlines the most important modifications made in MESOPUFF II and its processor programs. Each of these changes is discussed in detail in Chapter 2. MESOPAC II supplements twice-daily rawinsonde data with hourly surface data to construct wind fields at two levels. The greater temporal and spatial resolution of the surface data allows improved treatment of plume transport. Wind fields are determined at two user-selected levels; a lower level to represent boundary layer flow and an upper level to represent flow above the boundary layer.

The additional information contained in the surface meteorological observations allows calculation of important micrometeorological variables that determine the structure of the boundary layer (i.e., surface friction velocity,  $u_*$ , convective velocity scale,  $w_*$ , Monin-Obukhov length,  $L$ , and boundary layer height,  $z_i$ ). These variables are computed by MESOPAC II from surface meteorological data and surface characteristics (i.e., land use, roughness length) provided by the user for each grid point.

MESOPUFF II has been expanded to accommodate up to five pollutants: sulfur dioxide ( $\text{SO}_2$ ), sulfate ( $\text{SO}_4^{=}$ ), nitrogen oxides ( $\text{NO}_x = \text{NO} + \text{NO}_2$ ), nitric acid ( $\text{HNO}_3$ ), and nitrate ( $\text{NO}_3^-$ ). Chemical transformation rate expressions have been developed from the results of photochemical model simulations over a wide range of environmental conditions. The rate expressions include gas phase  $\text{NO}_x$  oxidation, and gas/aqueous phase  $\text{SO}_2$  oxidation. The  $\text{HNO}_3/\text{NH}_3/\text{NH}_4\text{NO}_3$  chemical equilibrium relationship has also been incorporated into the model.

The dry deposition of pollutants is treated in MESOPUFF II with a resistance model. The pollutant flux is proportional to the inverse of a sum of resistances of pollutant transfer through the atmosphere to the surface. The resistances depend on the characteristics of the pollutant, the underlying surface, and atmospheric conditions. MESOPUFF II contains options for the commonly used source depletion method of pollutant removal by dry deposition (i.e., pollutant is removed from the entire depth of the puff) or the more realistic surface depletion treatment (i.e., material is removed only from the surface layer) with a 3-layer submodule.

TABLE 1. MAJOR FEATURES OF MESOPUFF II

- Uses hourly surface meteorological data and upper air rawinsonde data
- Wind fields constructed for two layers (within boundary layer, above boundary layer)
- Boundary layer structure parameterized in terms of micrometeorological variables  $u^*$ ,  $w^*$ ,  $z_i$ ,  $L$
- Up to five species (e.g.,  $SO_2$ ,  $SO_4^{=}$ ,  $NO_x$ ,  $HNO_3$ ,  $NO_3^-$ )
- Space- and time-varying chemical transformations
- Space- and time-varying dry deposition; resistance model; source or surface depletion
- Space and time-varying wet removal
- Efficient puff sampling function.

Precipitation scavenging is frequently the dominant pollutant removal mechanism during precipitation periods. MESOPUFF II contains a scavenging ratio formulation for wet removal. The scavenging ratio depends on both the type and rate of precipitation, and the characteristics of the pollutant.

Improvements in MESOPUFF II have been made in the method which evaluates and sums the contributions of individual puffs to the total concentration. The model uses an integrated form of the puff sampling function that eliminates the problem of insufficient puff overlap commonly encountered with puff superposition models. This development allows continuous plumes to be accurately simulated with fewer puffs, thereby saving computational time and reducing computer storage requirements.

#### 1.4 Tennessee Plume Study

The TPS was conducted in August 1978 as part of EPA's Sulfur Transport and Transformation in the Environment (STATE) program. The experimental study was conducted in the vicinity of the TVA Cumberland Steam Plant. The Cumberland Plant is a base load 2600 MW plant which is located in northwestern Tennessee. Although sampling the Cumberland plume was the main objective of the experiment, plume measurements from other TVA plants (e.g., Johnsonville, Paradise and Gallatin) were made when they were transported near the Cumberland plume. The trajectory of the Cumberland plume was determined by tracking tetroons, a manned LAMP balloon, and ground and airborne sampling of a tracer gas ( $\text{SF}_6$ ). Dispersion and chemical measurements were obtained by aircraft and ground-based mobile vans. Four specific scenarios were studied:

- Vertical mixing during highly convective conditions to downwind distances of 50 km.
- Horizontal plume spread during stable conditions with significant wind shear to downwind distances of 300-500 km. The initial plume is emitted into the mixed layer.
- Dispersion during stable conditions to distances of 400 km. The initial plume is emitted into a stable layer.

- Dispersion and chemical changes over a diurnal cycle, with fumigation in the morning and layering in the evening.

Although a detailed evaluation of MESOPUFF II with the TPS data base is beyond the scope of the current study, a demonstration run for a two-day period during the TPS has been made. The purposes of the demonstration run were to allow a preliminary assessment of the  $\text{SO}_2$  to  $\text{SO}_4^=$  chemical transformation formulation for one of the scenarios (Scenario 4) and to qualitatively demonstrate the behavior of several other model algorithms.

## SECTION 2

### TECHNICAL DEVELOPMENTS

#### 2.1 Wind Fields

A principal concern in long range transport modeling is the spatial and temporal resolution of the data used to construct the wind field for plume advection. The spatial resolution of routinely available NWS rawinsonde data is only marginally adequate for long range transport modeling. The typical distance between rawinsonde stations is 300-500 kilometers. Another limitation is the poor temporal resolution of the routinely available twice-daily sounding data. Important variations in the wind field, mixing height, and atmospheric stability occur on much smaller space- and time-scales than those resolvable by the NWS upper-air sounding network.

To increase the spatial and temporal resolution of the meteorological data used in MESOPUFF II and to obtain a better representation of the boundary layer flow, the meteorological preprocessor program has been modified to allow the twice-daily upper air data to be supplemented with hourly surface data from the much denser network of NWS surface stations. In addition, wind fields are constructed at two levels: a lower level field representing boundary layer flow, and an upper level wind field representing flow above the boundary layer. The lower level winds are used to advect puffs within the mixed layer and to determine the plume rise of newly released puffs. The upper level winds are used to advect puffs which are above the boundary layer. At each time step, the appropriate wind field for advection of a puff is determined by comparison of the height of the puff center with the spatially and temporally varying mixing height. If the puff center is above (below) the mixing height at the closest grid point, the entire puff is advected with the upper (lower) level wind.

Considerable flexibility is allowed in choosing the most appropriate level or vertically-averaged layer for each wind field. Table 2 contains the available options. The default instructions are to use the winds averaged through the mixed layer for the lower level wind field, and the wind averaged from the top of the mixed layer through the 700 mb level ( $\sim 3000$  m) for the upper level wind field. However, if desired, the user may select other levels to determine the wind fields (e.g., surface and 850 mb levels). The model may be made a single wind field model by specifying the lower and upper wind fields to be the same.

The mixed layer averaged winds are calculated from twice-daily rawinsonde data from upper air stations and hourly surface data from the typically much denser network of surface stations. Layer-averaged wind speed and wind direction computed from the rawinsonde data are used to adjust the hourly surface winds. The following five step procedure, adapted from Draxler (1979), is used to determine the mixed layer wind at each point:

- (1) A representative rawinsonde sounding (00 or 12 GMT) is selected based upon the stability class at the nearest surface station to the grid point and the time of day. Neutral/unstable and stable conditions are assumed to be represented by the 00 GMT and 12 GMT sounding, respectively.
- (2) Using the sounding selected in Step (1), vertically averaged  $u$  (easterly) and  $v$  (northerly) wind components are computed through the layer from the surface to the grid point mixing height.
- (3) The ratio,  $R$ , of the layer-averaged wind speed to the surface wind speed at the rawinsonde station, and the angular difference in wind direction,  $\Delta\theta$ , between the layer averaged and surface winds are calculated.
- (4) The hourly surface wind data are used to calculate spatially interpolated surface wind components ( $u_s$ ,  $v_s$ ) at each grid point. Data from all surface stations within a user-specified

TABLE 2. OPTIONS FOR LOWER AND UPPER WIND FIELDS

<u>Option</u>	<u>Meteorological Data</u>
<b>Vertically Averaged Winds</b>	
Surface to mixing ht (1)	Surface, Rawinsonde
Mixing ht to 850 mb	Rawinsonde
Mixing ht to 700 mb (2)	Rawinsonde
Mixing ht to 500 mb	Rawinsonde
<b>Single Level Winds</b>	
Surface	Surface
850 mb	Rawinsonde
700 mb	Rawinsonde
500 mb	Rawinsonde

---

<sup>1</sup>Default lower level wind field

<sup>2</sup>Default upper level wind field

'scan-radius' of a grid point are used to compute  $(u_s, v_s)$  according to

$$(u_s, v_s)_{ij} = \frac{\sum_k \frac{\alpha_s}{r_s^2} \cdot (u_k, v_k)}{\sum_k \frac{\alpha_s}{r_s^2}} \quad (2-1)$$

- where  $u_s, v_s$  are the easterly and northerly components of the surface wind at grid point  $(i, j)$ ,  
 $u_k, v_k$  are the easterly and northerly components of the surface wind at surface station  $k$ ,  
 $r_s$  is the distance from the surface station to grid point  $(i, j)$ , and  
 $\alpha_s$  is an alignment weighting factor ( $\alpha_s = 1 - 0.5 |\sin \phi_s|$ , where  $\phi_s$  is the angle between the observed wind direction and the line from the surface station to the grid point).  
 For equal values of  $r_s$ , alignment weighting causes winds at a station directly upwind or downwind of a grid point to be weighted twice as heavily as the winds for a station at right angles to the grid point.
- (5) The mixed layer averaged wind at the grid point is calculated by multiplying the surface wind speed at the grid point from Step (4) by the wind speed ratio,  $R$ , at the nearest rawinsonde site. Similarly, the surface wind direction is adjusted by the wind direction factor,  $\Delta\theta$ .

The surface wind components in Step (4) must be computed each hour regardless of the choice of wind fields because these winds are also required in the calculation of the micrometeorological parameters described in Section 2.2.

Vertically averaged winds from the mixing height to the 850 mb, 700 mb or 500 mb levels are computed in the following manner. The 00 GMT and 12 GMT winds at each rawinsonde station are first interpolated in time, and then vertically averaged through the layer from the grid point mixing height to the selected level (e.g., 700 mb). The winds at grid point (i, j) are obtained by Equation (2-1), with the summation over rawinsonde stations instead of surface stations. Only rawinsonde stations within a 'scan-radius' of the grid point are considered. The mixing height must be lower than the pressure level that defines the top of the layer, otherwise, an error message is printed and execution of the program is terminated.

If one of the single-level upper air wind fields (e.g., 850 mb, 700 mb, or 500 mb) is chosen, only the wind data at the selected level is used to construct the wind field. For example, the 850 mb wind at each grid point is calculated by interpolating the 850 mb winds at each rawinsonde station over time, and then applying Equation (2-1) with the summation over the rawinsonde stations.

## 2.2 Micrometeorological Parameters

Boundary layer turbulence is generated by convective and mechanical processes. Convective or buoyancy-induced turbulence is produced by a positive (upward) heat flux at the ground which is driven by solar heating. Mechanical mixing originates from shear-induced turbulence which is caused by frictional interaction of the wind with the earth's surface. The structure of the boundary layer can be described in terms of a small number of micrometeorological variables; the surface sensible heat flux,  $H$ , the surface friction velocity,  $u_*$ , and the boundary layer height,  $z_i$ . Many studies (e.g., Deardorff and Willis 1975, van Ulden 1978) have shown the importance of these and related parameters in boundary layer meteorology. MESOPAC II uses simple empirical relationships to estimate micrometeorological parameters from routinely available meteorological measurements. Vertical dispersion and dry deposition of pollutants are parameterized in MESOPUFF II in terms of these variables. Horizontal and

near-field vertical puff growth continue to use dispersion formulas which require classification of stability into PGT classes.

The following sections describe the methods used to obtain the micrometeorological parameters needed by MESOPUFF II from routinely available meteorological data.

### 2.2.1 Surface Friction Velocity

The surface friction velocity,  $u_*$ , can be computed from routinely available meteorological data if the surface roughness characteristics are known. First, the sensible heat flux is calculated from an estimate of net radiation. Then  $u_*$  is determined from the wind speed, surface roughness,  $z_0$ , and heat flux.

The sensible heat flux,  $H$ , is estimated during daylight hours by the following equations (Maul 1980):

$$H = \alpha R + H_0 \quad (2-2)$$

$$R = 950 \beta \sin v \quad (2-3)$$

$$H_0 = 2.4 C - 25.5 \quad (2-4)$$

where,

- $H$  is the sensible heat flux ( $Wm^{-2}$ ),
- $H_0$  is the heat flux in the absence of solar incoming radiation ( $Wm^{-2}$ ),
- $\alpha$  is a land use constant, ( $\sim 0.3$ ),
- $R$  is the incoming solar radiation ( $Wm^{-2}$ ),
- $\beta$  is a radiation reduction factor due to the presence of clouds,
- $v$  is the solar elevation angle, and
- $C$  is the opaque cloud cover (in tenths).

Table 3 contains default values for the solar radiation reduction factor ( $\beta$ ) due to the different cloud amounts. The values of  $\beta$  are adapted from those used by Maul (1980).

The sine of the solar elevation angle,  $\sin \nu$ , is given by:

$$\sin \nu = \sin \phi \sin K_d + \cos \phi \cos K_d \cos H_A \quad (2-5)$$

$$H_A = (\pi/12) (\tau - E_m) - \lambda \quad (2-6)$$

$$E_m = 12. + 0.12357 \sin (D) - 0.004289 \cos (D) \\ + 0.153809 \sin (2D) + 0.060783 \cos (2D) \quad (2-7)$$

$$D = (d-1) (360./365.242)(\pi/180) \quad (2-8)$$

$$K_D = \sin^{-1} (0.39784989 \sin (\pi \sigma_A/180)) \quad (2-9)$$

$$\sigma_A = 279.9348 + D(180/\pi) + 1.914827 \sin (D) \\ - 0.079525 \cos (D) + 0.019938 \sin (2D) - 0.00162 \cos (2D) \quad (2-10)$$

where  $\phi$  is the latitude (radians),  
 $\lambda$  is the longitude (radians),  
 $d$  is the Julian day, and  
 $\tau$  is the time of day (hours).

With the above estimate of  $H$ , the surface friction velocity,  $u_*$ , can be estimated during unstable conditions by the method described by Wang and Chen (1980):

$$u_* = \tilde{u}_* \{1 + a \ln [1 + b Q_o/\tilde{Q}_o]\} \quad (2-11)$$

$$\tilde{u}_* = \frac{ku_m}{\ln (z_m/z_o)} \quad (2-12)$$

TABLE 3. SOLAR RADIATION REDUCTION FACTOR  $\beta$

<u>Cloud Cover (Tenths)</u>	<u><math>\beta</math></u>
0	1.00
1	0.91
2	0.84
3	0.79
4	0.75
5	0.72
6	0.68
7	0.62
8	0.53
9	0.41
10	0.23

$$z_m = z_{ms} - 4 z_o \quad (2-13)$$

$$Q_o = H/(\rho c_p) \quad (2-14)$$

$$\tilde{Q}_o = \frac{\theta \tilde{u}_*^3}{k g z_m} \quad (2-15)$$

$$a = \begin{cases} 0.128 + 0.005 \ln (z_o/z_m) & z_o/z_m \leq 0.01 \\ 0.107 & z_o/z_m > 0.01 \end{cases} \quad (2-16)$$

$$b = 1.95 + 32.6 (z_o/z_m)^{0.45} \quad (2-17)$$

where,

- k is the von Karman constant ( $\sim 0.4$ ),
- $c_p$  is the specific heat of air at constant pressure ( $996 \text{ m}^2/(\text{s}^2 \text{ deg})$ ),
- $u_*$  is the surface friction velocity (m/s),
- $u_m$  is the wind speed (m/s) measured at height  $z_{ms}$  (m),
- $z_o$  is the surface roughness (m), and
- $\rho$  is the density of air ( $\text{kg/m}^3$ ).

During stable conditions,  $u_*$  is determined by the following method (Venkatram 1980):

$$u_* = \frac{C_{DN} u_m}{2} [1 + C^{0.5}] \quad (2-18)$$

$$C_{DN} = \frac{k}{\ln (z_m/z_o)} \quad (2-19)$$

$$C = 1 - \frac{4 u_o^2}{C_{DN} u_m^2} \quad C \geq 0 \quad (2-20)$$

$$u_o^2 = \frac{\gamma z_m}{k A} \quad (2-21)$$

where  $\gamma$  and  $A$  are constants with values of 4.7 and 1100, respectively, and  $C_{DN}$  is the neutral drag coefficient.

### 2.2.2 Monin-Obukhov Length

The Monin-Obukhov length,  $L$ , is defined as:

$$L \equiv - \frac{u_*^3 T_o}{g k Q_o} \quad (2-22)$$

where  $T_o$  is the observed air temperature and  $g$  is the acceleration due to gravity. During unstable conditions,  $L$  is calculated directly from its definition using values of  $u_*$  and  $Q_o$  derived earlier. During stable conditions,  $L$  is given by Venkatram (1980b) as:

$$L = 1100 u_*^2 \quad (2-23)$$

### 2.2.3 Mixed Layer Height

During daylight hours, solar radiation reaching the ground produces a positive (upward) flux of sensible heat and the development of a well-mixed adiabatic layer. If the hourly variation of  $H$  is known, the mixed layer height,  $z_i$ , at time  $t + 1$  can be estimated from  $z_i$  at time  $t$  in a stepwise manner (Maul 1980).

$$(z_1)_{t+1} = \left[ (z_i)_t^2 + \frac{2H(1+E)\Delta t}{\psi_1 \rho c_p} - \frac{2(\Delta\theta)_t(z_i)_t}{\psi_1} \right]^{1/2} + \frac{(\Delta\theta)_{t+1}}{\psi_1} \quad (2-24)$$

$$(\Delta\theta)_{t+1} = \left( \frac{2\psi_1 E H \Delta t}{\rho c_p} \right)^{1/2} \quad (2-25)$$

where

- $\psi_1$  is the potential temperature lapse rate in the layer above  $z_i$ ,
- $\Delta t$  is the time step (3600 s),
- $E$  is a constant ( $\sim 0.15$ ), and
- $\Delta\theta$  is the temperature discontinuity at the top of the mixed layer.

The lapse rate,  $\psi_1$ , is determined through a layer  $\Delta z$  meters above the previous hour's convective mixing height. For daytime hours up to 23 GMT, the morning (12 GMT) sounding at the nearest rawinsonde station is used to calculate  $\psi_1$ . After 23 GMT, the evening (00 GMT) sounding is used. To avoid computational problems,  $\psi_1$  is not allowed to be less than 0.001 °K/m.

The neutral (shear produced) boundary layer height is given by Venkatram (1980) as:

$$z_i = \frac{B u_*}{(f N_B)^{1/2}} \quad (2-26)$$

- where  $f$  is the Coriolis parameter,
- $B$  is a constant ( $\sqrt{2}$ ), and
- $N_B$  is the Brunt-Vaisala frequency in the stable layer aloft.

The daytime mixing height is the maximum of the convective and mechanical values predicted by Equations 2-25 and 2-26.

In the stable boundary layer, mechanical turbulence production determines the vertical extent of dispersion. Venkatram (1980b) provides the following empirical relationship to estimate  $z_i$  during stable conditions.

$$z_i = 2400 u_*^{3/2} \quad (2-27)$$

#### 2.2.4 Convective Velocity Scale

During convective conditions, turbulence is generated primarily by the sensible heat flux originating from the ground. The appropriate velocity scale during these conditions is the convective velocity,  $w_*$ .

$$w_* \equiv \left( \frac{g}{T_o} Q_o z_i \right)^{1/3} \quad (2-28)$$

The convective velocity can be calculated directly from its definition, since  $Q_o$  and  $z_i$  have been determined from Equations 2-14 and 2-24, respectively.

### 2.3 Dry Deposition - Three-Layer Model

The rate at which pollutants are deposited at the surface depends on many factors: the state of the atmosphere, the characteristics of the surface, and the properties of the pollutant. For example, the rate of deposition can sometimes be limited by the rate of pollutant transfer to the surface by atmospheric diffusion processes. Due to the importance of vegetation as a sink for atmospheric pollutants, the structure of the canopy and the physiological state of the vegetation are also important factors. The properties of a pollutant such as its solubility, molecular diffusivity and for larger particles, the size and shape of the particles are additional factors that influence the rate of deposition. Table 4 contains a listing

**TABLE 4. FACTORS INFLUENCING DRY DEPOSITION REMOVAL RATES**

<u>Micrometeorology variables</u>	<u>Depositing Material</u>		<u>Surface Variables</u>
	<u>Particles</u>	<u>Gases</u>	
Aerodynamic roughness:	Agglomeration	Chemical activity	Accommodation:
-Mass transfer	Diameter	Diffusion:	-Exudates
(a) Particles	Density	-Brownian	-Trichomes
(b) Gases	Diffusion:	-Eddy	-Pubescence
-Heat	-Brownian	Partial pressure in equilibrium with surface	-Wax
-Momentum	-Eddy equal to	Solubility	Biotic surfaces
Atmospheric stability	(a) Particle		Canopy growth:
Diffusion, effect of:	(b) Momentum		-Dormant
-Canopy	(c) Heat		-Expanding
-Diurnal variation	-Effect of canopy on		Senescent
-Fetch	Diffusiophoresis		Canopy Structure:
Flow separation:	Electrostatic effects:		-Areal density
-Above canopy	-Attraction		-Bark
-Below canopy	-Repulsion		-Bole
Friction velocity	Gravitational settling		-Leaves
Inversion layer	Hydroscopicity		-Porosity
Pollutant concentration	Impaction		-Reproductive structure
Relative humidity	Interception		-Soils
Seasonal variation	Momentum		-Stem
Solar radiation	Physical properties		-Type
Surface heating	Resuspension		Electrostatic properties
Temperature	Shape		Leaf-vegetation:
Terrain:	Size		-Boundary Layer
-Uniform	Solubility		-Change at high winds
-Nonuniform	Thermophoresis		-Flutter
Turbulence			-Stomatal resistance
Wind velocity			Non-biotic surfaces
Zero-plane displacements:			pH effects on:
-Mass transfer			-Reaction
(a) Particles			-Solubility
(b) Gases			Pollutant penetration and distribution in canopy
-Heat			Prior deposition loading
-Momentum			Water

From: Sehmel (1980)

compiled by Sehmel (1980) of the variables believed to be most important in influencing dry deposition rates.

The dry flux of a pollutant can be written (Slinn et al. 1978) as:

$$F_d = F_z + v_g C \quad (2-29)$$

where

$F_d$  is the total (downward) dry flux,  
 $F_z$  is the turbulent and molecular diffusive flux,  
 $v_g$  is the average drift velocity due to gravitational settling and phoretic effects, and  
 $C$  is the pollutant concentration.

For larger particles (diameters  $>1 \mu\text{m}$ ), gravitational settling and particle inertia become increasingly important effects. Brownian diffusion dominates the mass transfer of gases and small particles (diameters  $<0.1 \mu\text{m}$ ) in the near surface quasi-laminar layer. As shown in Figure 3, a minimum in deposition velocity is observed from particles in the range  $0.1\text{--}1.0 \mu\text{m}$  where these mechanism are less effective (Hicks 1982). Most models of dry deposition use the concept of a deposition velocity (Chamberlain and Chadwick 1953) to express the total dry flux:

$$F_d = v_d C \quad (2-30)$$

where  $v_d$  is the deposition velocity (including both gravitational and diffusive effects) at a reference height.

Due to the number and variability of the factors influencing deposition rates, reported deposition velocities exhibit considerable variability. For example,  $\text{SO}_2$  deposition velocities summarized by Sehmel (1980) range over two orders of magnitude (Figure 4). Although it is not possible to include the effects of all the variables listed in Table 4 in determining  $v_d$ , it is possible to improve upon the assumption commonly used in mesoscale models

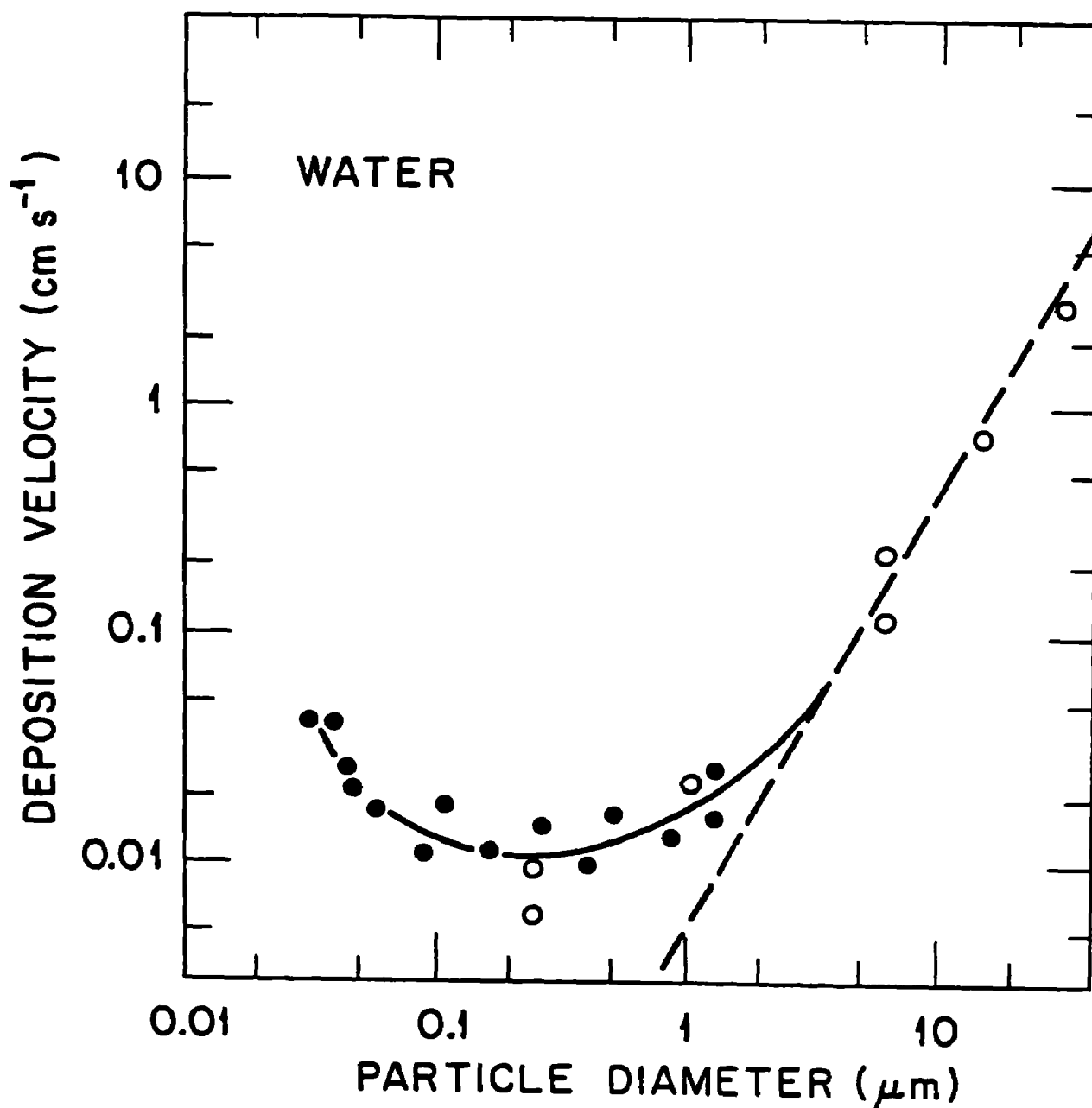


Figure 3 Particle Deposition to Water Surfaces. Solid Circles are Due to Moller and Schumann (1979), Open Circles to Sehmel and Sutter (1973). The Dashed Line at the Right Represents the Terminal Settling Speed for 1.5 g cm<sup>-3</sup> Particles. Source: Hicks (1982)

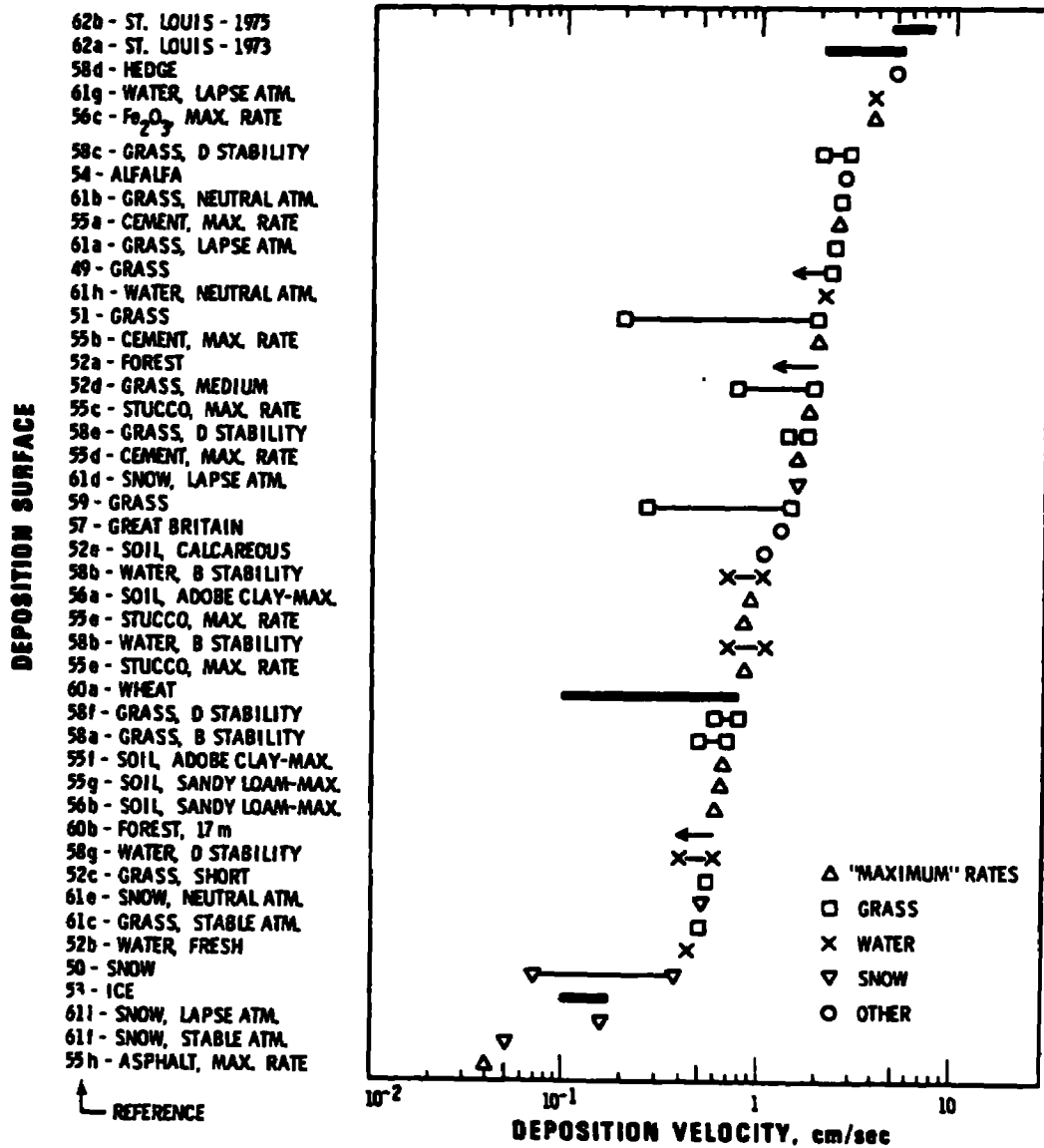


Figure 4  $\text{SO}_2$  Deposition Velocities  
 Source: Sehmel (1980)

of spatially and temporally constant deposition velocities. In MESOPUFF II, the deposition velocity is expressed as the inverse of a sum of resistances to transfer of the pollutant through the atmosphere to the surface.

$$v_d = (r_a + r_s + r_c)^{-1} \quad (2-31)$$

where  $r_a$  is the aerodynamic resistance (s/m),  
 $r_s$  is the surface resistance (s/m), and  
 $r_c$  is the canopy resistance (s/m).

The aerodynamic resistance is the resistance to pollutant transfer through the atmospheric surface layer. It is a function of wind speed, atmospheric stability, and surface roughness. Except for very large particles, the aerodynamic resistance for gases and particles is the same. The surface resistance represents the resistance to transfer across the quasi-laminar layer surrounding smooth surfaces. Wind tunnel studies have shown that the thickness of this layer is typically about 50  $\mu\text{m}$  (Hicks 1982). However, surface roughness elements can sometimes penetrate this layer, providing an alternative route for the transfer. Therefore,  $r_b$  is an average value of this resistance. The canopy resistance is the resistance to transfer within the surface or plant constituting the final resting place for the pollutant. The canopy resistance depends on the characteristics of the pollutant (e.g., solubility) as well as the physiological properties of the vegetation.

The aerodynamic resistance,  $r_a$ , is given by Wesely and Hicks (1977) as:

$$r_a = (k u_*')^{-1} [\ln(z_s/z_o) - \psi_H] \quad (2-32)$$

$$\psi_H = \begin{cases} -5z_s/L & 0 < z_s/L < 1 \\ \exp [0.598 + 0.39 \ln(-z_s/L) - 0.090 \{\ln(-z_s/L)\}^2] & -1 < z_s/L < 0 \end{cases} \quad (2-33)$$

where  $z_s$  is the reference height (10 meters in MESOPUFF II),  
 $z_0$  is the surface roughness length (m),  
 $u_*$  is the friction velocity (m/s),  
 $\psi_H$  is a function accounting for stability effects,  
 $k$  is the von Karman constant, and  
 $L$  is Monin-Obukhov length (m).

The surface resistance,  $r_s$ , can be expressed (Wesely and Hicks 1977)  
as:

$$r_s = (k u_*)^{-1} k B^{-1} \quad (2-34)$$

where  $B^{-1}$  is the surface transfer coefficient.

For  $SO_2$ ,  $k B^{-1} = 2.6$  (Wesely and Hicks 1977). The other gaseous pollutants in MESOPUFF II (e.g.,  $NO_x$ ,  $HNO_3$ ) are assumed to have similar values of  $k B^{-1}$ . For particles,  $r_s$  is a complex function of many factors. Depending upon the pollutant size distribution, particle inertia and gravitational settling effects may be important. Given current uncertainties regarding  $r_s$  for particles,  $r_s$  is simply assumed constant for  $SO_4^{2-}$  and  $NO_3^-$  with a default value of 10 s/cm. Although Wesely and Hicks (1977) suggest  $r_s$  may be as low as 1 s/cm, the larger value is presently used in the model to be consistent with deposition velocities of  $\sim 0.1$  cm/s found in other studies (e.g., Garland 1978) for sulfate.

Shieh et al. (1979) estimate canopy resistance for  $SO_2$  as a function of land use and stability class for summertime conditions. These values, contained in Table 5, are used as default values in MESOPUFF II. It should be noted that these values are based only on expected midsummer conditions. More appropriate values (e.g., for snow covered surfaces) may be entered for model applications during other seasons.

Based upon its high solubility and reactivity,  $r_c$  for  $HNO_3$  is assumed equal to zero (Hicks 1982). Canopy resistance for  $NO_x$  are

TABLE 5. SUMMERTIME SO<sub>2</sub> CANOPY RESISTANCES AS A  
FUNCTION OF LAND USE TYPE AND STABILITY CLASS

Category	Land Use Type	$z_o$ (m)	Stability Class			
			A,B,C	D	E	F
1	cropland and pasture	0.20	100.	300.	1000.	0.
2	cropland, woodland and grazing land	0.30	100.	300.	1000.	0.
3	irrigated crops	0.05	100.	300.	1000.	0.
4	grazed forest and woodland	0.90	100.	300.	1000.	0.
5	ungrazed forest and woodland	1.00	100.	300.	1000.	0.
6	subhumid grassland and semiarid grazing land	0.10	100.	300.	1000.	0.
7	open woodland grazed	0.20	100.	300.	1000.	0.
8	desert shrubland	0.30	200.	500.	1000.	1000.
9	swamp	0.20	50.	75.	100.	0.
10	marshland	0.50	75.	300.	1000.	0.
11	metropolitan city	1.00	1000.	1000.	1000.	0.
12	lake or ocean	10 <sup>-4</sup>	0.	0.	0.	0.

From: Shieh, Wesely, and Hicks (1979).

1.3 s/cm (A-C stability), 5 s/cm (D stability), and 15 s/cm (E-F stability). Uptake of the particles  $\text{SO}_4^-$  and  $\text{NO}_3^-$  by plant stomata is less relevant; therefore, total resistance for  $\text{SO}_4^-$  and  $\text{NO}_3^-$  is determined by  $r_a$  and  $r_s$  (i.e.,  $r_c = 0$ ).

With knowledge of the concentration and the deposition velocity, the pollutant flux is determined by Equation 2-30. MESOPUFF II has two options for treating the removal of pollutant from a puff. The first option is the commonly used source depletion approximation. This method assumes that material deposited is removed from the full depth of the puff. The change in mass is:

$$Q(t+1) = Q(t) \exp \left[ - \frac{v_d \Delta t}{\Delta s} \int_s^{s + \Delta s} g(s') ds' \right] \quad (2-35)$$

Where  $Q(t)$ ,  $Q(t+1)$  is the mass (g) of pollutant in the puff at the beginning and end of the time step,  
 $s$ ,  $s + \Delta s$  is the position of the puff at the beginning and end of the time step, and  
 $g(s)$  is the vertical term of the Gaussian puff equation as given by Equation 2-59. For a puff uniformly mixed in the vertical,  $g(s) = 1/z_i$ .

The source depletion model effectively enhances the rate of vertical diffusion of the pollutant because mass removed at the surface is immediately replaced with material from above. However, in the atmosphere, the rate of deposition can be limited (usually only during stable conditions) by the rate of pollutant mass transfer through the boundary layer to the surface layer. This overall boundary layer resistance is not included in the aerodynamic resistance. Horst (1977) suggests that the source depletion model may introduce a bias in the deposition flux. Excessively high deposition fluxes and concentrations may be predicted by the source depletion model in the near-field, and as a result, the concentrations and deposition fluxes may be underpredicted further

downwind. This effect is illustrated in Figure 5 where the source depletion model results are compared to those of the surface depletion model of Horst (1977).

To account for the effect of boundary layer mixing, MESOPUFF II has the option to treat puffs that have become vertically well-mixed with a 3-layer model (see Figure 6). The surface layer is a shallow layer (10 m) next to the ground that rapidly adjusts to changes in surface conditions. Pollutants in the middle layer are uniformly mixed up to the top of the current boundary layer. The upper layer consists of pollutant material above the boundary layer dispersed upward during previous turbulent activity. The pollutant flux into the surface layer is:

$$\text{Flux} = \kappa (C_m - C_s) / (z_i - z_s) = v_d C_s \quad (2-36)$$

where  $\kappa$  is an overall boundary layer eddy diffusivity ( $\text{m}^2/\text{s}$ ),  
 $C_m$  is the concentration in the middle layer, and  
 $C_s$  is the concentration at the top of the surface layer.

During stable conditions,  $\kappa$  is given by Brost and Wyngaard (1978) as:

$$\kappa = k_1 u_* z_i \quad (2-37)$$

and during neutral or unstable conditions  $\kappa$  is:

$$\kappa = \text{Maximum} \{k_1 u_* z_i, k_2 w_* z_i\} \quad (2-38)$$

The constants  $k_1$  and  $k_2$  have default values of 0.01 and 0.1, respectively.

The term  $v_d C_s$  can be written as  $v_d' C_m$ , where  $v_d'$  is an effective deposition velocity taking into account boundary layer mass transfer.

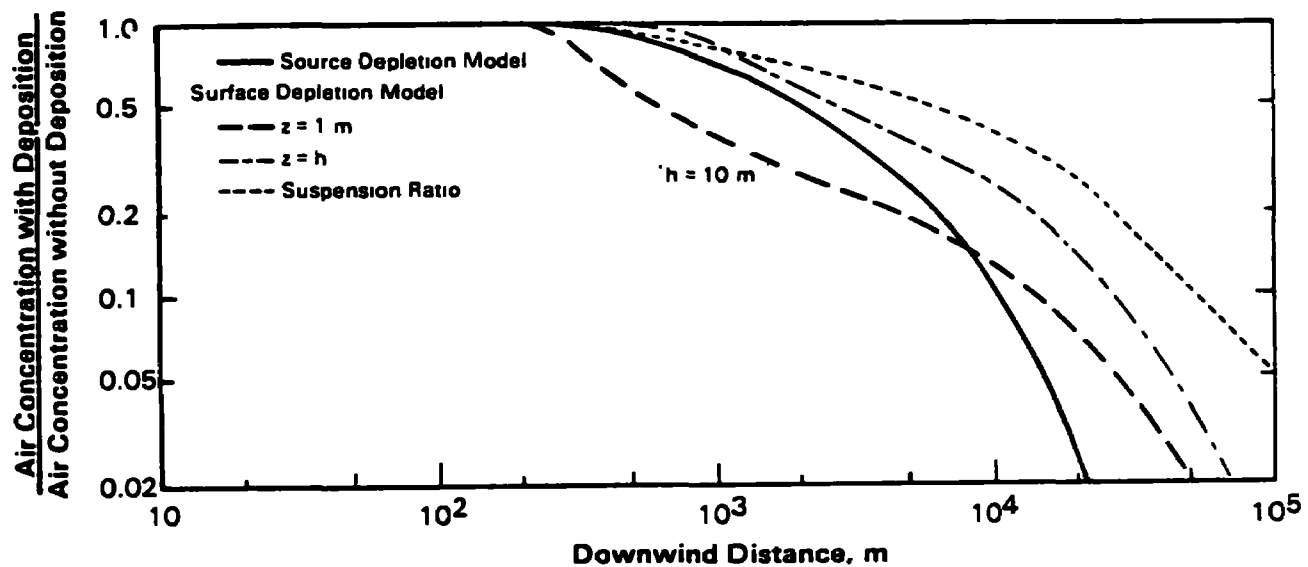


Figure 5 Comparison of Source Depletion and Surface Depletion Models. For  $v_d/u = 10^{-2}$ , Stable Thermal Stratification (F Stability) from Horst (1977)

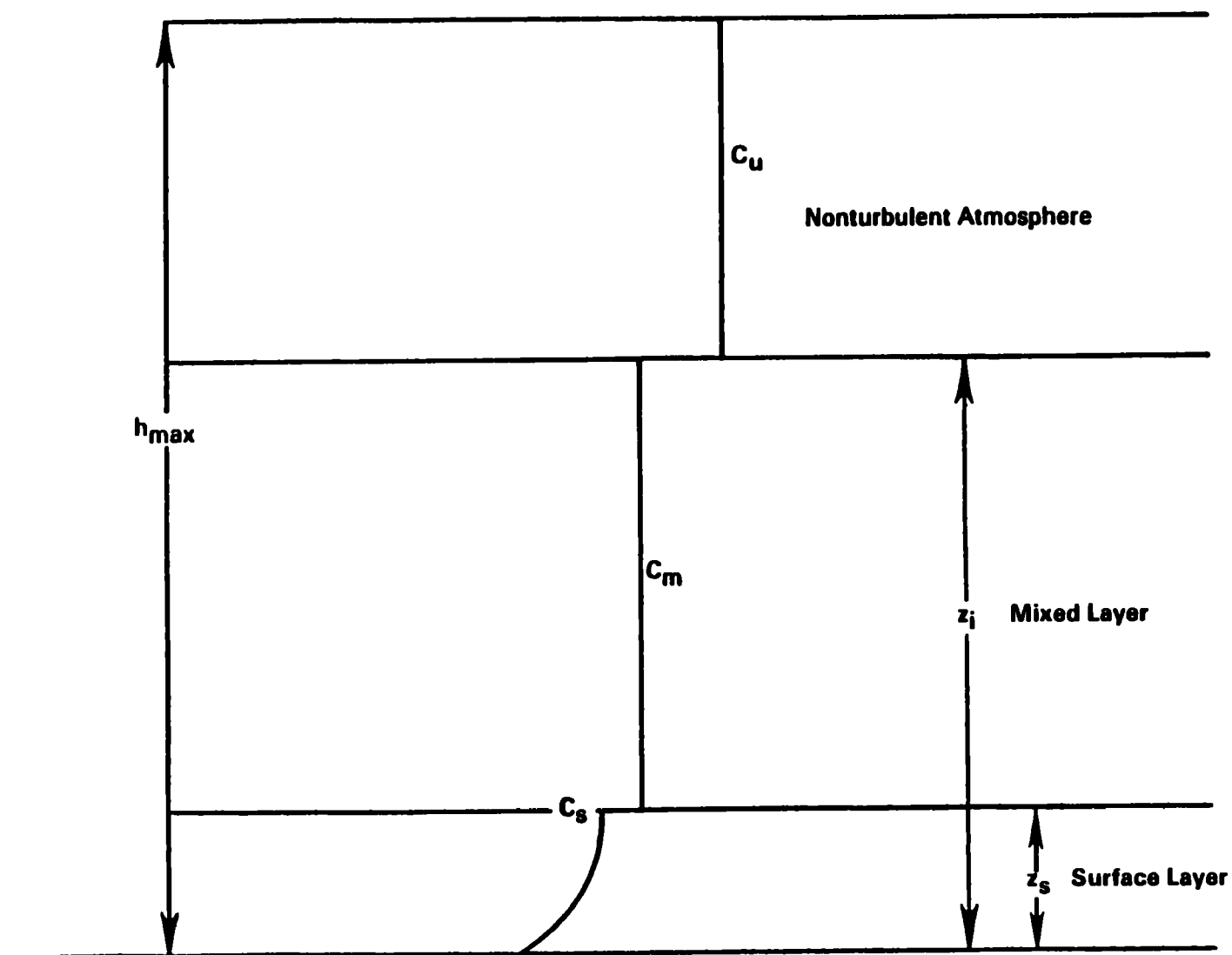


Figure 6 Optional Three Layer System Used in MESOPUFF II

$$v_d' = \frac{\kappa v_d}{\kappa + v_d(z_i - z_s)} \quad (2-39)$$

In the 3-layer model, only material in the surface layer is available for deposition at the surface. The effective deposition velocity,  $v_d'$ , is used to evaluate the change in pollutant mass in the puff due to dry deposition. The model predictions are those corresponding to  $C_s$  in Figure 6.

## 2.4 Chemical Transformations

The accuracy of air quality models for chemically reactive species depends strongly on the chemical submodel, as well as the transport, diffusion, and deposition formulations. The fidelity of atmospheric chemical mechanisms is often limited by the availability of kinetic and mechanistic data for the species of concern and sometimes the model's structure. For example, often the atmospheric chemistry of emitted compounds depends on numerous other compounds formed and destroyed in other chemical reactions. Not only are the rate constants and products uncertain for many of these reactions, but also the model's formulation may not allow for inclusion of intermediate species and/or second-order reactions. The latter is true for the puff transport/dispersion formulation used in the MESOPUFF II model. Thus, chemical mechanisms for models such as MESOPUFF II must be formulated as pseudo-first-order reactions. The accuracy of the first-order reaction mechanism may be enhanced by parameterization of the rate constants so as to reflect the characteristics of the higher-order reaction system.

The chemical process of concern for the MESOPUFF II model are the conversions of sulfur dioxide ( $SO_2$ ) to sulfate aerosol ( $SO_4^{2-}$ ) and oxides of nitrogen ( $NO_x$ ) to nitrate aerosol ( $NO_3^-$ ). Although the atmospheric chemistry of these compounds has been studied for nearly two decades, substantial uncertainties exist in the current chemical knowledge of  $SO_x$  and  $NO_x$  reaction pathways and rates under ambient conditions.

Laboratory and field studies have shown that chemical transformation rates for these species can vary several orders of magnitude under different environmental conditions (Calvert et al. 1978; Wilson 1981; Richards et al. 1981; Newman 1981). It is, therefore, important for the chemical submodel to incorporate the dependency of transformation rates on environmental conditions.

A first order reaction mechanism consisting of the following reactions has been formulated for MESOPUFF II:



The rate constants have been parameterized in terms of environmental conditions such as solar radiation, relative humidity, temperature, and background ozone concentrations. The parameterizations have been developed from laboratory data, field data, and analysis of nonlinear chemical mechanisms for  $\text{SO}_x$  and  $\text{NO}_x$  oxidation. The following subsections describe the rationale for and development of the MESOPUFF II chemical transformation scheme.

#### 2.4.1 Chemical Pathways for Sulfate and Nitrate Aerosol Formation

Research performed during the last twenty years has identified many of the important pathways for  $\text{SO}_2$  and  $\text{NO}_x$  oxidation. Laboratory and field studies have shown fine particulate matter to be a major product of  $\text{SO}_2$  oxidation and a minor product of  $\text{NO}_x$  oxidation under ambient conditions. Figures 7 and 8 illustrate the chemical pathways for  $\text{SO}_2$  and  $\text{NO}_x$  oxidation, and aerosol formation. Oxidation may occur by gas and aqueous

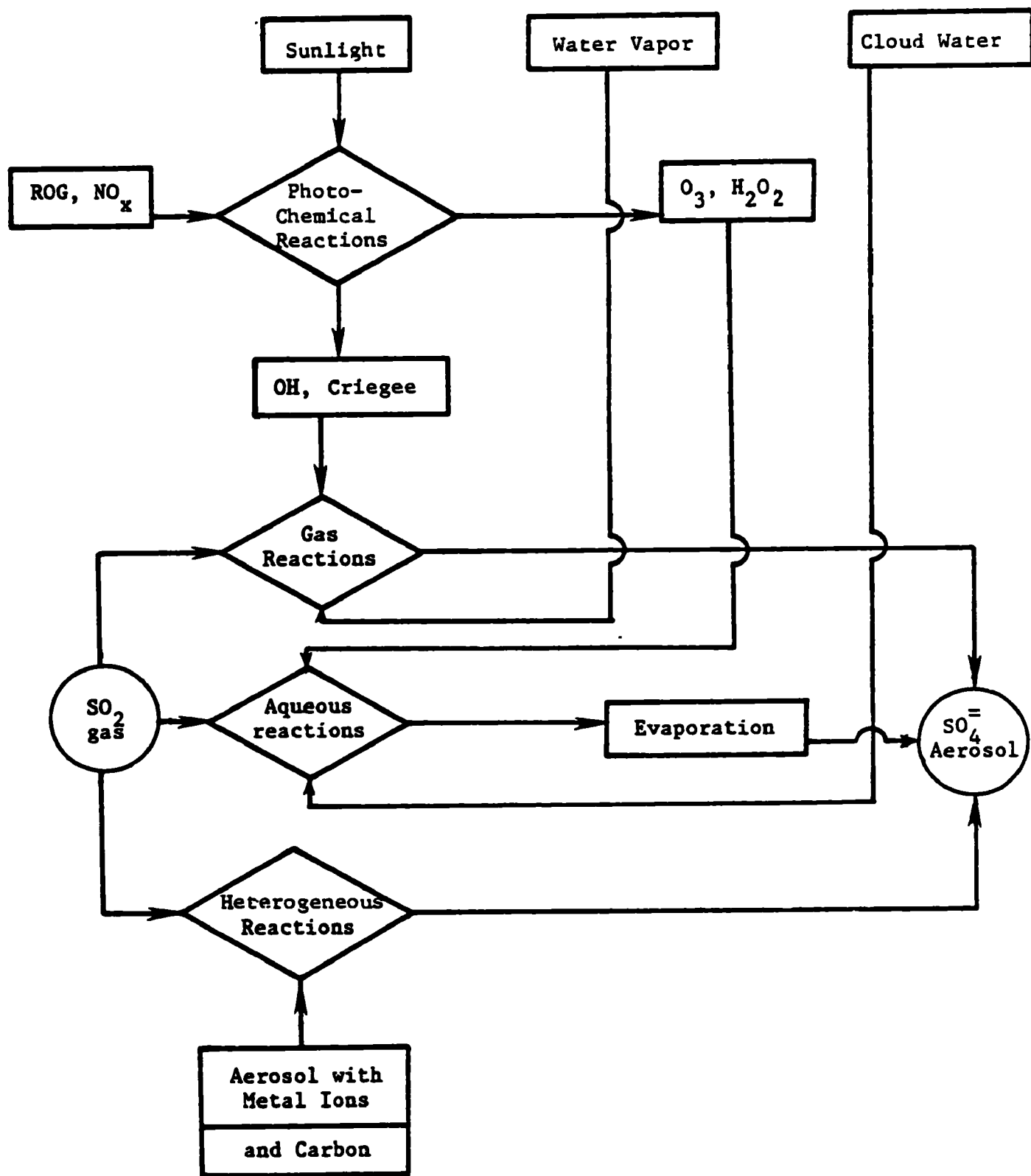
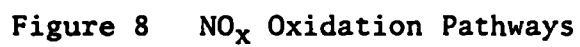


Figure 7  $\text{SO}_2$  Oxidation Pathways



phase reactions. The gas phase reactions for both  $\text{SO}_x$  and  $\text{NO}_x$  involve free radical photochemistry and, thus, are coupled to the oxidation of reactive organic gases (ROG). The aqueous phase oxidation reactions for  $\text{SO}_x$  and  $\text{NO}_x$  are less well understood than the gas phase reactions, however, photochemical products such as ozone ( $\text{O}_3$ ) and hydrogen peroxide ( $\text{H}_2\text{O}_2$ ) are believed to be the principal oxidants for  $\text{SO}_2$ .

Homogenous gas phase reactions are believed to be the dominant  $\text{SO}_2$  oxidation pathway in the presence of sunlight and absence of clouds or fog (Calvert et al. 1978). Three of the most important reactions for  $\text{SO}_2$  are:



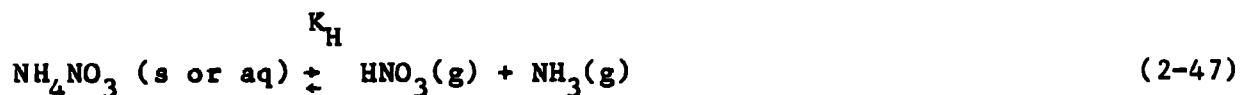
In the presence of trace amounts of water vapor,  $\text{HSO}_3$  and  $\text{SO}_3$  rapidly form a sulfate aerosol or attach to pre-existing aerosols. Reactions of  $\text{HSO}_3$  with  $\text{NO}$  in the presence of  $\text{O}_2$  may occur but the mechanism remains uncertain (Calvert et al. 1978). The reaction with the hydroxyl radical ( $\text{OH}$ ) is believed to be most important. The reactions with the Criegee biradicals, formed from ozone-alkene reactions, may be important at high alkene concentrations in urban environments (Atkinson and Lloyd 1980). These reactions can produce  $\text{SO}_2$  oxidation rates of up to 5% per hour.

$\text{SO}_2$  oxidation may also occur via reactions of the dissolved  $\text{S(IV)}$  constituents, primarily bisulfate and sulfite, with dissolved ozone and hydrogen peroxide ( $\text{H}_2\text{O}_2$ ) (Maahs 1982; Penkett et al. 1979). The aqueous phase oxidation may also be catalyzed by  $\text{Mn}^{++}$ ,  $\text{Fe}^{++}$ , and/or elemental carbon (Martin 1982). Recent reviews suggest that oxidation by  $\text{H}_2\text{O}_2$  may be the dominant process under acidic conditions (Schwartz 1982). Although there is considerable uncertainty whether  $\text{H}_2\text{O}_2$  production in the gas or aqueous phase is sufficient to sustain this reaction, relatively small amounts of  $\text{H}_2\text{O}_2$  can produce transformation rates of up to 100% per hour

locally in cloud or rain water. Since cloud water is believed to be recycled (condensed-evaporated) rapidly, the aqueous phase reactions may be an important pathway for sulfate aerosol formation under cloudy or foggy conditions (Hegg and Hobbs 1981).

The oxidation of  $\text{NO}_x$  is strongly dependent on gas phase  $\text{ROG/NO}_x/\text{O}_3$  photochemistry and is generally more rapid than  $\text{SO}_2$  oxidation. As shown in Figure 8,  $\text{NO}_x$  can be oxidized to nitric acid ( $\text{HNO}_3$ ) and organic nitrates ( $\text{RNO}_3$ ) including oxygenated nitrates such as peroxyacetylnitrate (PAN). Nitric acid formation occurs primarily by the reaction of  $\text{NO}_2$  with OH (at a rate  $\sim 8$  times faster than  $\text{SO}_2 + \text{OH}$ ). Oxidation of  $\text{NO}_x$  to  $\text{N}_2\text{O}_5$  (with involvement of  $\text{O}_3$ ) followed by a heterogeneous reaction with water and reactions of  $\text{NO}_3$  with aromatic hydrocarbons may also lead to  $\text{HNO}_3$  formation.  $\text{HNO}_3$  is, in turn, destroyed very slowly by photolysis and reaction with OH.

Nitric acid combines with ammonia gas to form solid or aqueous ammonium nitrate ( $\text{NH}_4\text{NO}_3$ ). Unlike  $\text{SO}_4^{=}$  formation, the  $\text{NO}_3^-$  formation process is reversible. Equilibrium is established between nitric acid, ammonia, and ammonium nitrate:



The equilibrium constant

$$K_H = \frac{[\text{NH}_3][\text{HNO}_3]}{[\text{NH}_4\text{NO}_3]} \quad (2-48)$$

is dependent on temperature and relative humidity in a nonlinear manner as shown in Figure 9 (Stelson and Seinfeld 1982). The equilibrium constant can vary several orders of magnitude over a typical diurnal cycle. Given fixed amounts of total nitrate, ammonia, and water vapor, higher  $\text{NH}_4\text{NO}_3$  concentrations are expected at night, due to lower nighttime temperature and

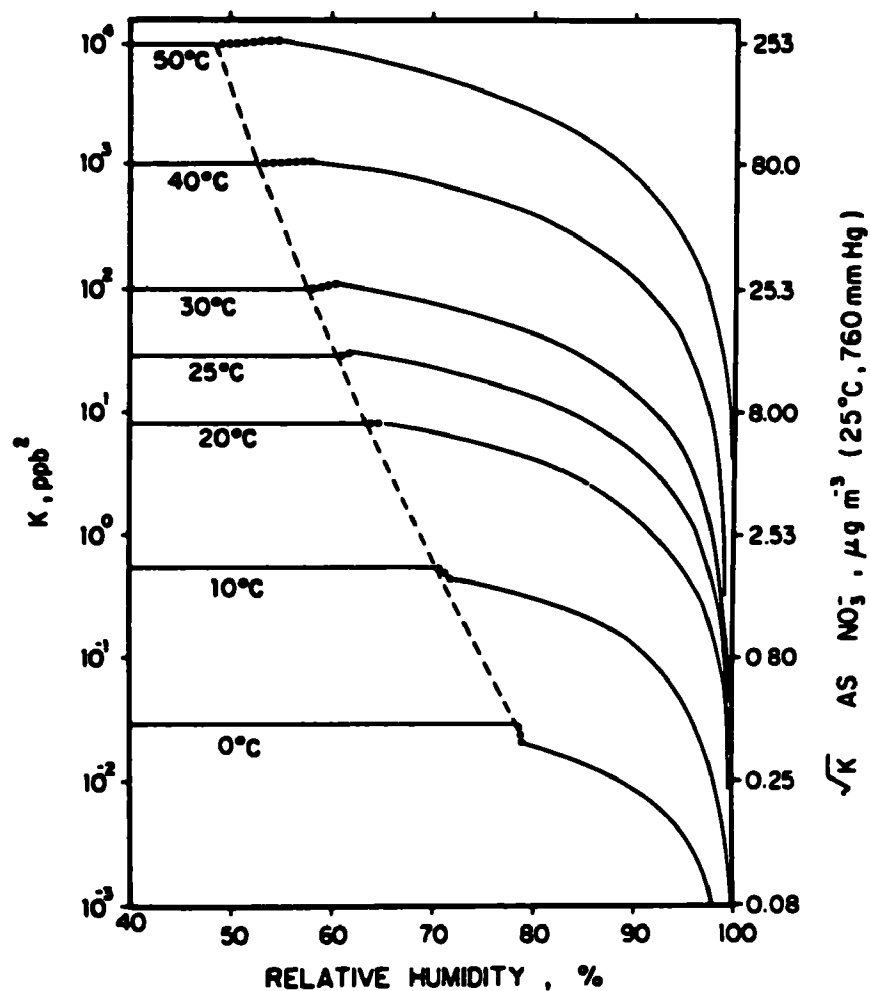


Figure 9  $\text{NH}_4\text{NO}_3$  Dissociation Constant Temperature and Relative Humidity Dependence  
Source: Stelson and Seinfeld (1982)

higher relative humidity. Thus, the nitrate aerosol cannot be considered a stable product like sulfate. Also, unlike  $\text{SO}_4^{=}$ , its ambient concentrations are limited by the availability of ammonia which is preferentially scavenged by sulfate (Stelson et al. 1983).

The formation of organic nitrate such as peroxyacetylnitrate (PAN) and PAN analogs is the second major pathway for  $\text{NO}_x$  oxidation. The organic nitrates are formed primarily by reactions of  $\text{NO}_2$  with  $\text{RCO}_3$  radicals (such as acetylperoxy). Organic nitrates may also be formed by reactions of  $\text{NO}$  with  $\text{RO}_2$  radicals and  $\text{NO}_2$  with  $\text{RO}$  radicals. The  $\text{RCO}_3$  radicals are formed from acetaldehyde and higher aldehydes which are emitted directly by sources and photochemically formed from organic gases. PAN formation rates are, therefore, strongly dependent on hydrocarbon loadings. The stability of PAN, and therefore, its net formation rate, strongly depends on temperature. PAN decomposes into  $\text{NO}_2$  and  $\text{RCO}_3$  at a rate which increases with temperature. This has lead many scientists to view PAN as more of a temporary reservoir for  $\text{NO}_2$  than a permanent sink. The results of multi-day simulations of  $\text{HC/NO}_x/\text{O}_3$  systems with diurnally varying temperature and radiation performed at ERT suggest the cumulative formation of PAN greatly exceeds its decomposition, hence we believe PAN is a major  $\text{NO}_x$  sink. However, in contrast to the  $\text{HNO}_3$  pathway, there is no evidence of nitrate aerosol formation from PAN.

Little is known regarding aqueous phase oxidation of dissolved  $\text{NO}_2$  to  $\text{NO}_3^-$ .  $\text{NO}_2$  has low solubility and at this time the only reaction of importance involves  $\text{S(IV)aq} + \text{N(III)aq}$  (Schwartz and White 1982; Martin et al. 1981). Its reaction products are unknown. Based on the current information, the aqueous phase oxidation pathways appears to be far less important than the gas phase oxidation pathway for  $\text{NO}_x$ .

#### 2.4.2 Development of a Pseudo-First Order Reaction Mechanism

Rate constant expressions for reactions 1-3 (Equations 2-40 to 2-42) were developed to represent  $\text{SO}_2$  and  $\text{NO}_x$  oxidation under different environmental conditions. The gas and aqueous components of the  $\text{SO}_2$

oxidation rate were developed separately. Only gas phase oxidation was considered for  $\text{NO}_x$ . The  $\text{HNO}_3/\text{NH}_3/\text{NH}_4\text{NO}_3$  equilibrium relationship (Equation 2-43) was incorporated directly into the mechanism. Since the gas phase chemistry for  $\text{SO}_2$  and  $\text{NO}_x$  is better understood than the aqueous phase, greater emphasis was placed on developing the gas component of the psuedo-first order rate expressions.

Since the oxidation of  $\text{SO}_2$  and  $\text{NO}_x$  depends strongly on gas phase photochemistry, rate expressions were derived from the results of photochemical model simulations. A variable volume Lagrangian photochemical box model was exercised over a wide range of environmental conditions. The model was designed to simulate plume gases dispersing into and reacting with background air. The Atkinson et al. (1982) photochemical mechanism was employed for the calculations. It incorporates the important gas phase reaction pathways for the  $\text{ROG}/\text{NO}_x/\text{SO}_x$  chemical system shown in Appendix A.

Five groups of parameters expected to influence photooxidation rates of plume gases were allowed to vary in the photochemical model runs. These surrogate parameters included season, background reactivity, dispersion conditions, time of emissions release, and plume  $\text{NO}_x$  loadings. A total of 144 model runs were made representing parameter combinations for 3 different seasons, 4 different background reactivities, 2 different dispersion conditions, 2 different times of emissions release, and 3 different plume  $\text{NO}_x$  loadings.

Solar radiation and ambient temperature data for the photochemical model runs varied with season. Diurnally varying clear sky solar radiation for a latitude of  $40^\circ$  and daily average temperatures of 30, 20 and  $10^\circ\text{C}$  were employed for the summer, fall, and winter seasons, respectively. The background air concentrations included 11 classes of ROG compounds and ozone. The background ROG concentrations of 0.05, 0.25, 0.50, 2.0 ppmC were employed. The composition of ROG was assumed to be 60% reactive alkanes, 10% alkenes, 25% aromatics, and 5% aldehydes on a carbon basis in all cases. Background ozone concentrations were varied between 0.02 and

0.20 ppm. Plume  $\text{NO}_x$  loadings were varied from 0.007 to 1.4 ppm. Relative humidity of 60% and a constant initial  $\text{SO}_2$  concentration of 2.0 ppm were employed for all the calculations. All parameter values used for the simulation are summarized in Table 6.

The runs generated a data base with 1224 hourly conversion rates and associated environmental conditions. The data base included the conversion rate of  $\text{SO}_2$  to  $\text{SO}_4^=$ ,  $\text{NO}_x$  to all products and  $\text{NO}_x$  to nitric acid. The solar radiation and concentrations of  $\text{NO}_x$ , ROG, and  $\text{O}_3$  at the midpoint of the hour were stored along with the time, temperature, stability, release time, etc. for each hour.

Stepwise linear regression on the logarithms of the output variables was performed to determine the controlling variables and the best regression equations. Solar radiation, background ozone concentrations, and atmospheric stability were found to be important parameters controlling daylight gas phase  $\text{SO}_2$  oxidation rates. Background ozone concentration, atmospheric stability, and  $\text{NO}_x$  concentrations were found to be most highly correlated with the predicted  $\text{NO}_x$  oxidation rates. The following hourly transformation rate expressions were determined:

$$k_{1G} = 36 R^{0.55} \text{OZ}^{0.71} S^{-1.29} \text{ (gas component)} \quad (2-49)$$

$$k_2 = 1206 \text{OZ}^{1.50} S^{-1.41} \text{NOX}^{-0.33} \quad (2-50)$$

$$k_3 = 1261 \text{OZ}^{1.45} S^{-1.34} \text{NOX}^{-0.12} \quad (2-51)$$

where  $k_{1G}$  is  $\text{SO}_2$  to  $\text{SO}_4^=$  transformation rate (% per hour);  
 $k_2$  is  $\text{NO}_x$  to  $\text{HNO}_3 + \text{RNO}_3$  transformation rate (% per hour)\*;  
 $k_3$  is  $\text{NO}_x$  to  $\text{HNO}_3$  (only) transformation rate (% per hour);

---

\*The rate constant for  $\text{NO}_x \rightarrow \text{RNO}_3$  is  $k_2 - k_3$ .

TABLE 6. PARAMETER VARIATIONS IN THE PHOTOCHEMICAL MODELING SIMULATIONS

<u>Surrogate Parameter</u>	<u>Number of Variations</u>	<u>Model Input Parameters and Variations</u>
Season	3	Ambient temperature and solar radiation varied with season. Ambient temperatures of 30, 20, and 10°C were employed for the summer, fall, and winter cases, respectively. Diurnally varying clear sky solar radiation for 40° latitude in the 3 seasons were employed.
Background Air Reactivity	4	Background air concentrations of ozone and ROG were varied together to represent background air reactivity. Background ozone concentrations were assumed to be correlated with season. Ozone concentrations of 0.02, 0.05, 0.08, and 0.20 ppm were employed for summer. Fall and winter ozone concentrations equal to 75 and 50% of the summer values were employed. The corresponding four ROG concentrations employed were 0.05, 0.25, 0.50, and 2.0 ppmC. The composition of the ROG was assumed to be 60% reactive alkanes, 10% alkenes, 25% aromatics, and 5% aldehydes.
Dispersion	2	The rate of plume dilution varied with atmospheric stability and wind speed. A stable case with 1.5 m/sec wind speed and a slightly unstable case with 5 m/sec wind speed were assumed. Dilution rates were based on the time rate of change of plume cross-sectional area ( $\sigma_y \sigma_z$ ) from an initial area of 10,000 m.
Release Time	2	Sunrise and noon time were used as emission release times.
Plume NO <sub>x</sub> Loading	3	Initial (at $\sigma_y \sigma_z = 10^4 \text{ m}^2$ ) plume NO <sub>x</sub> concentrations of 0.007, 0.35, and 1.40 ppm were employed. The NO <sub>x</sub> was partitioned as 90% NO and 10% NO <sub>2</sub> on a volume basis.

$R$  is total solar radiation ( $\text{kWatt/m}^2$ );  
 $OZ$  is background ozone concentration (ppm);  
 $S$  is atmospheric stability index ranging from 2 to 6 (e.g., 2 for PGT stability classes A and B, 4 for class D, and 6 for class F);  
 $NO_x$  is ambient  $NO_x$  concentration (ppm), minimum value is  $10^{-4}$  ppm.

The correlation coefficients ( $R^2$ ) for these regression equations are 0.80, 0.89, and 0.87, respectively, which indicate good correlations.

The dependency of these transformation expressions on environmental parameters is consistent with physical expectations. The rates are inversely proportional to the stability index which is consistent with the expectation that higher background air entrainment rates (i.e., low stability index) should result in higher conversion rates. They are proportional to the background ozone concentration. Since ozone can be thought of as a surrogate for OH concentration, this is consistent with expectations from the gas phase chemistry. The  $SO_2$  rate expression is also dependent on solar radiation. Since the rate of the photolytic reactions, which generate the free radicals, depend directly on the radiation intensity, this result is expected. The  $NO_x$  expression has a weak inverse dependence on the  $NO_x$  concentration which is consistent with the expectation that higher  $NO_x$  concentration impedes oxidation rates. A similar dependence was expected for the  $SO_2$  oxidation rates. However, the statistical analysis indicated  $NO_x$  concentration was not nearly as significant as the three other parameters in the  $SO_2$  rate expression.

An aqueous phase  $SO_2$  conversion rate expression was determined empirically. Since the amount of aqueous phase S(IV) available for conversion depends on the amount of water present (as well as condensation/evaporation rates and  $SO_2$  solubility which in turn depends on pH, etc.), relative humidity was selected as a commonly available surrogate for liquid water content. Although conversion may occur rapidly in the aqueous phase, only a small portion of the  $SO_2$  is in the aqueous phase. For this reason, a relatively low maximum aqueous oxidation rate (to be applied to  $SO_2(g)$ ) was selected: three percent per hour. Since observations of  $SO_2/SO_4$

in plumes suggest overall oxidation rates increase dramatically at high relative humidity (Gillani et al. 1981) a higher order dependence on humidity was selected. The aqueous phase component of  $k_1$  is

$$k_{1A} = 3 \times 10^{-8} RH^4 \text{ (aqueous component)*} \quad (2-52)$$

where RH is the relative humidity (in percent). A minimum of 0.2% per hour is used for  $k_{1A}$ . The accuracy of this expression is highly uncertain. Depending on environmental conditions, such as the availability of hydrogen peroxide or metal catalysts, the actual conversion rate may be an order of magnitude higher or lower than indicated by the expression.

Other researchers have formulated  $SO_2$  oxidation rate expressions based on observations. Henry and Hidy (1981, 1982) employed principal component analysis of urban aerometric data to derive expressions for the homogeneous and heterogeneous components. This analysis showed that a large portion of the variance in  $SO_2$  oxidation rate was explained by the variance in ozone concentration. This photochemical component was generally much larger than the heterogeneous component. The following gas phase  $SO_2$  oxidation rate expressions (in % per hour) represent the average for all the stations examined:

$$k_1 = 34 [O_3] \text{ for St. Louis} \quad (2-53)$$

$$k_1 = 85 [O_3] \text{ for Los Angeles} \quad (2-54)$$

where  $[O_3]$  is the average hourly ozone concentration in ppm. These expressions generally predict  $SO_2$  oxidation rates greater than predicted by ERT expression.

---

\*NOTE:  $k_1 = k_{1G} + k_{1A}$ .

Gillani et al. (1981) derived a  $\text{SO}_2$  oxidation rate expression which is applicable when relative humidity is less than 75% based on plume chemistry studies. This expression is

$$k_1 = 0.03 R h [\text{O}_3] \quad (2-55)$$

where

$k_1$  is  $\text{SO}_2$  oxidation rate in % per hour,  
 $R$  is total solar radiation ( $\text{kw/m}^2$ ),  
 $h$  is plume depth (m) (minimum of  $z_i$  or  $3\sigma_z$ ), and  
 $[\text{O}_3]$  is background ozone concentration (ppm).

It is important to note that this expression identifies essentially the same variables controlling  $\text{SO}_2$  oxidation rate as the ERT expression. Figure 10 shows a comparison between  $\text{SO}_2$  oxidation rates predicted with the Gillani et al. and ERT expressions for a range of conditions. These conditions include 8, 10, and 12 A.M. clear sky radiation in summer, fall, and winter; ozone concentration of 0.02 to 0.12 ppm; and a range of stability/mixing heights. The results show the two expressions predict comparable (within  $\pm 30\%$ )  $\text{SO}_2$  oxidation rates. This result is quite significant since each equation was derived in an entirely different manner: Gillani et al. from observations, and ERT's from the kinetic model. The good agreement between the results provides additional confidence in both equations. However, since the ERT expression was generated from a wider range of conditions than the Gillani et al. expression, it is the preferred mechanism in MESOPUFF II.

The parameterized rate constant expressions discussed above apply only to daylight conditions. The gas phase free radical chemistry turns off at night. The expressions which employ ozone concentration and radiation levels as surrogate for OH concentration are inappropriate at night (Zak 1981). Nighttime oxidation of  $\text{SO}_2$  and  $\text{NO}_2$  to sulfates and nitrates, respectively, is believed to be slow due to the absence of OH. Observations of plume chemistry confirm this expectation. Figure 11 shows observed hourly conversion rates of  $\text{SO}_2$  to  $\text{SO}_4^=$  from eight plume studies as a

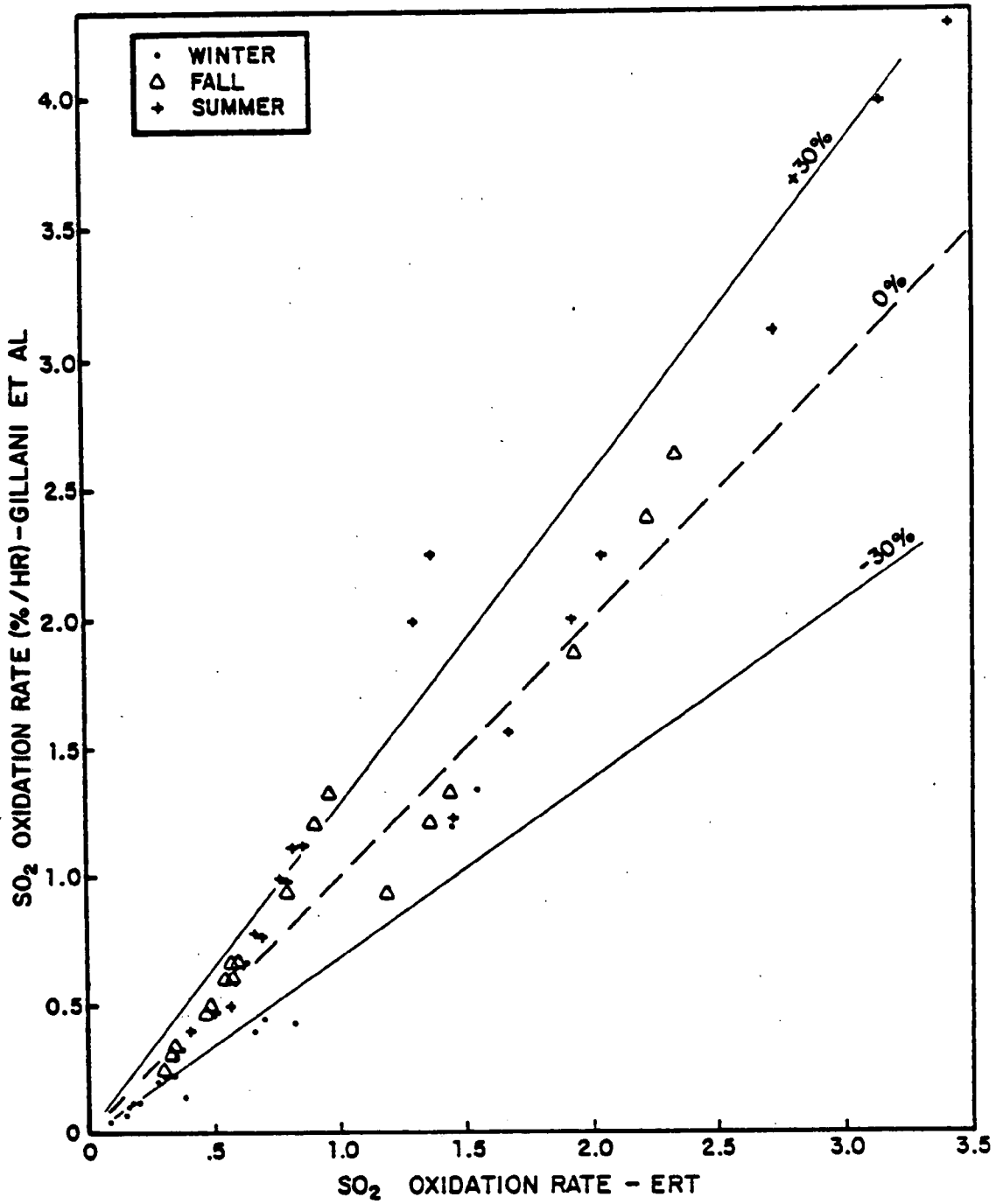


Figure 10 Comparison of  $\text{SO}_2$  Oxidation Rates (% per Hour) Predicted by the ERT and Gillani et al. Expressions

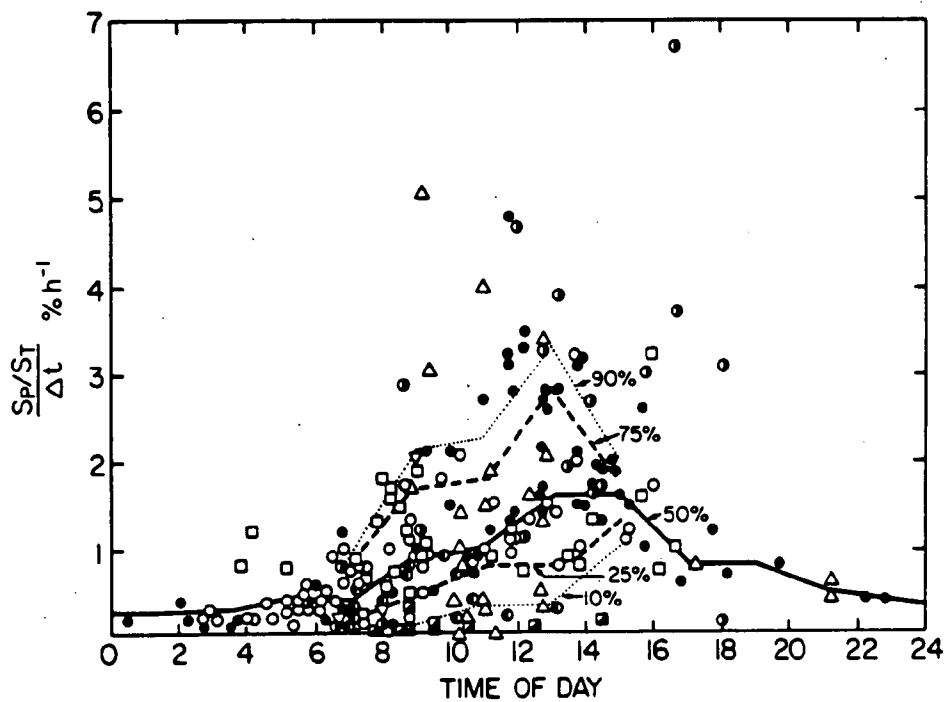


Figure 11 Average Plume Sulfur Conversion Rate as a Function of Mean Time of Day of Plume Transport. Only Data Corresponding to Plume Age Greater than 1.5 Hours are Plotted.  
Source: Wilson (1981)

function of time of day (Wilson 1981). These data show  $\text{SO}_2$  oxidation rates are generally less than 0.5% per hour at night. Observed nighttime  $\text{NO}_x$  oxidation rates are also low. Forrest et al. (1981) found  $\text{NO}_x$  to total inorganic nitrate conversion rates in plumes of 0.1 to 3% per hour at night and during early morning hours. These low oxidation rates are presumably the result of heterogeneous reactions. Since these reactions are not well understood and, in general, are less important than daytime oxidation rates, constant oxidation rates are used in the model at night. Based on the results of plumes studies, oxidation rates of 0.2 and 2% per hour for  $\text{SO}_2$  and  $\text{NO}_x$ , respectively, were selected for nighttime conditions in the MESOPUFF II chemical submodel.

#### 2.4.3 Implementation of Chemistry

It is important to design air quality models with flexibility and options to accommodate different applications and future improvements in scientific knowledge. Several options have been incorporated in the MESOPUFF II chemistry submodel to provide flexibility. First, in addition to the ERT expressions for  $\text{SO}_x$  and  $\text{NO}_x$  transformation rates, the submodel includes the Gillani et al. and Henry and Hidy expressions for  $\text{SO}_2$  oxidation rates as options. Second, the model includes the option for external (user) specification of hourly transformation rates of reactions 1-3 (Equations 2-40 to 2-42). The user also has the options to specify hourly ozone data from a network of stations, a single ozone concentration for all hours, or use the default value of 80 ppb. Similarly, the user may use the default  $\text{NH}_3$  concentration (10 ppb) and nighttime oxidation rates (see above) or specify values more appropriate for the application. Thus, the MESOPUFF II chemical submodel has ample flexibility to accommodate different applications and even different pollutants.

One of the problems in implementing chemistry in the puff modeling framework is that the model keeps track of puffs individually, yet atmospheric chemistry is a function of the concentrations from all puffs at a given location. This is particularly important for the  $\text{NO}_x$  chemistry, since the parameterized oxidation rate depends on  $\text{NO}_x$  concentration and

the  $\text{NH}_4\text{NO}_3$  concentration depends on the total  $\text{NH}_3$  and nitrate concentrations. Clearly, in a situation where puffs overlap, it would be incorrect to calculate the  $\text{NO}_x$  oxidation rate solely on the puff  $\text{NO}_x$  concentration and/or to calculate the particulate nitrate assuming all the ambient  $\text{NH}_3$  would be available for one puff. Thus, the model has been designed to employ the local average  $\text{NO}_x$  concentration from all puffs in the  $\text{NO}_x$  oxidation rate expression for a single puff and apply the  $\text{HNO}_3/\text{NH}_3/\text{NH}_4\text{NO}_3$  equilibrium relationship using the sum of total nitrate concentrations from all puffs and ammonia (total ammonia minus sulfate) at the location of interest.

## 2.5 Wet Removal

Numerous studies (e.g., Scott 1978, 1981; Garland 1978) have shown precipitation scavenging to be an efficient pollutant removal mechanism, especially for particulate pollutants such as  $\text{SO}_4^{=}$  that serve as cloud condensation nuclei. Wet removal of soluble and reactive gaseous pollutants such as  $\text{SO}_2$  and  $\text{HNO}_3$  is also very important. Plumes can be nearly completely washed out by moderate rainfall within a few hours. During precipitation events, wet removal can easily dominate dry deposition in pollutant removal. On an annual basis, the average wet removal rates for  $\text{SO}_2$  and  $\text{HNO}_3$  in Eastern North America and Europe are comparable to those due to dry deposition (Scriven and Fisher 1975; Levine and Schwartz 1982); for  $\text{SO}_4^{=}$  wet removal appears to be the more important removal mechanism (Scriven and Fisher 1975).

Wet removal includes both in-cloud scavenging (rainout) and below cloud scavenging (washout). The scavenging process is a complex one involving many factors. Scott (1978, 1981) has found precipitation scavenging of sulfate to be a strong function of the mechanism of precipitation formation and storm type (Figure 12). For example, the ratio of sulfate concentration in precipitation to that in air (i.e., the washout ratio, W) is 10-50 times larger for precipitation with growth due primarily to accretion than for precipitation growth due to vapor deposition. The scavenging efficiency of gases is a function of pollutant's solubility in water and reactivity.

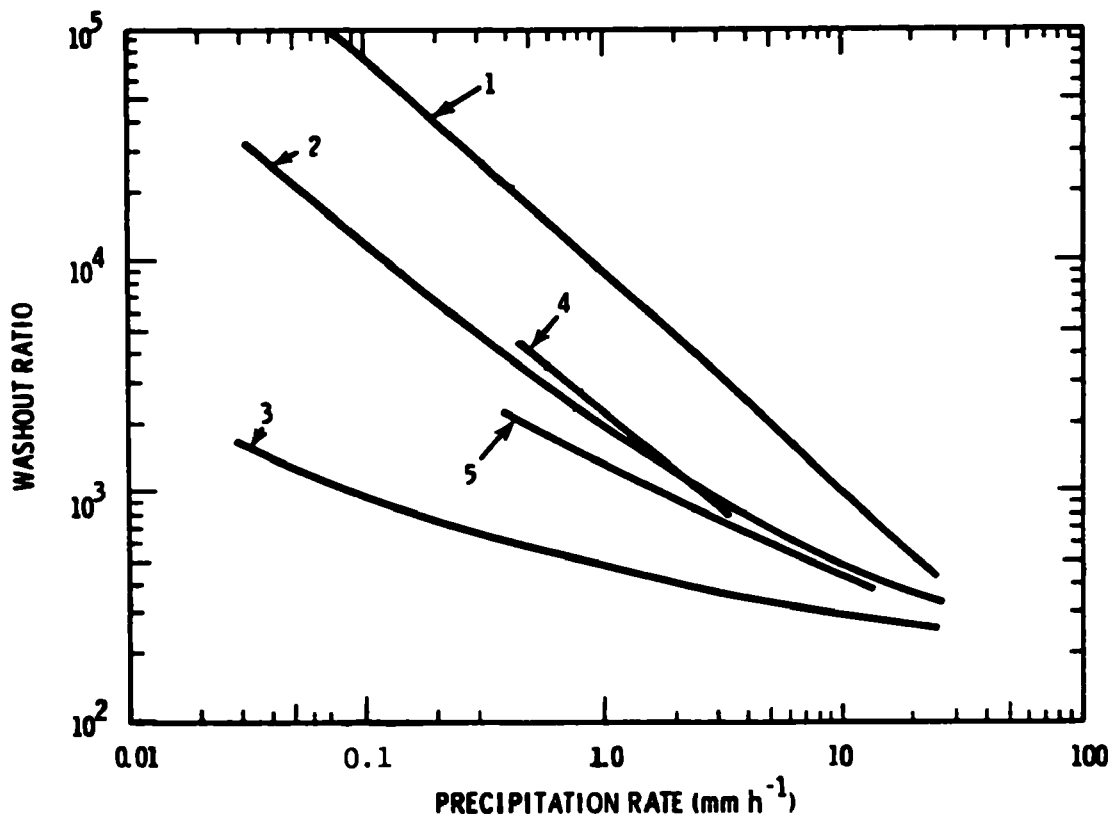


Figure 12 Washout Ratio as a Function of Precipitation Rate for Different Storm Types. Curve 1 Represents Predictions for Intense Convective Storms or from Clouds Whose Tops are Warmer than 0°C; Curve 2 Represents Predictions for Storms Where Rain Develops Without the Assistance of an Ice Growth Stage; Curve 3 is for Storms Where the Ice Growth Process is Necessary for Initiating Precipitation; Curve 4 is from Observed <sup>24</sup>Na Concentrations in Rainwater at Quillayute, Washington on 5, 6 April 1970; and Curve 5 is the Same as Curve 4 Except Curve for Data from 11 December 1969. Source: Scott (1978)

Barrie (1981) has shown  $\text{SO}_2$  washout ratios to be strongly dependent on the pH of the rain and temperature (Figure 13).

However, a simple parameterization of wet removal suitable for order of magnitude wet removal estimates and using only routinely available meteorological variables is required in MESOPUFF II. A convenient approach compatible with the puff superposition principle is the scavenging coefficient formulation:

$$Q(t + 1) = Q(t) \exp [- \Lambda \Delta t] \quad (2-56)$$

where  $Q(t)$ ,  $Q(t + 1)$  is the mass (g) of pollutant in the puff at the beginning and end of the time step,  
 $\Lambda$  is the scavenging ratio ( $\text{s}^{-1}$ ), and  
 $\Delta t$  is the time step (s).

Maul (1980) expresses  $\Lambda$  as:

$$\Lambda = \lambda (R/R_1) \quad (2-57)$$

where  $R$  is the rainfall rate (mm/hr),  
 $R_1$  is a reference rainfall rate of 1 mm/hr, and  
 $\lambda$  is a scavenging coefficient ( $\text{s}^{-1}$ ).

The rainfall rate used in Equation 2-57 is that observed at the closest surface station to the center of the puff. Table 7 contains the default values of the scavenging coefficient used in MESOPUFF II. Different values of  $\lambda$  are considered for liquid and frozen precipitation. Slinn et al. (1978) note that snow scavenging of gases is generally negligible. The scavenging coefficients for  $\text{SO}_2$  and  $\text{SO}_4^{=}$  removal by rain is based on Maul (1980) and Garland (1978). The scavenging coefficient for  $\text{NO}_3^-$  is believed to be roughly comparable to that for  $\text{SO}_4^{=}$ . Maul (1980) showed that values of  $\lambda \sim 3-6 \times 10^{-5} \text{ s}^{-1}$  can be derived for sulfate with the assumption of full removal from air entrained into the clouds. The high solubility and reactivity of  $\text{HNO}_3$  suggests that a scavenging coefficient

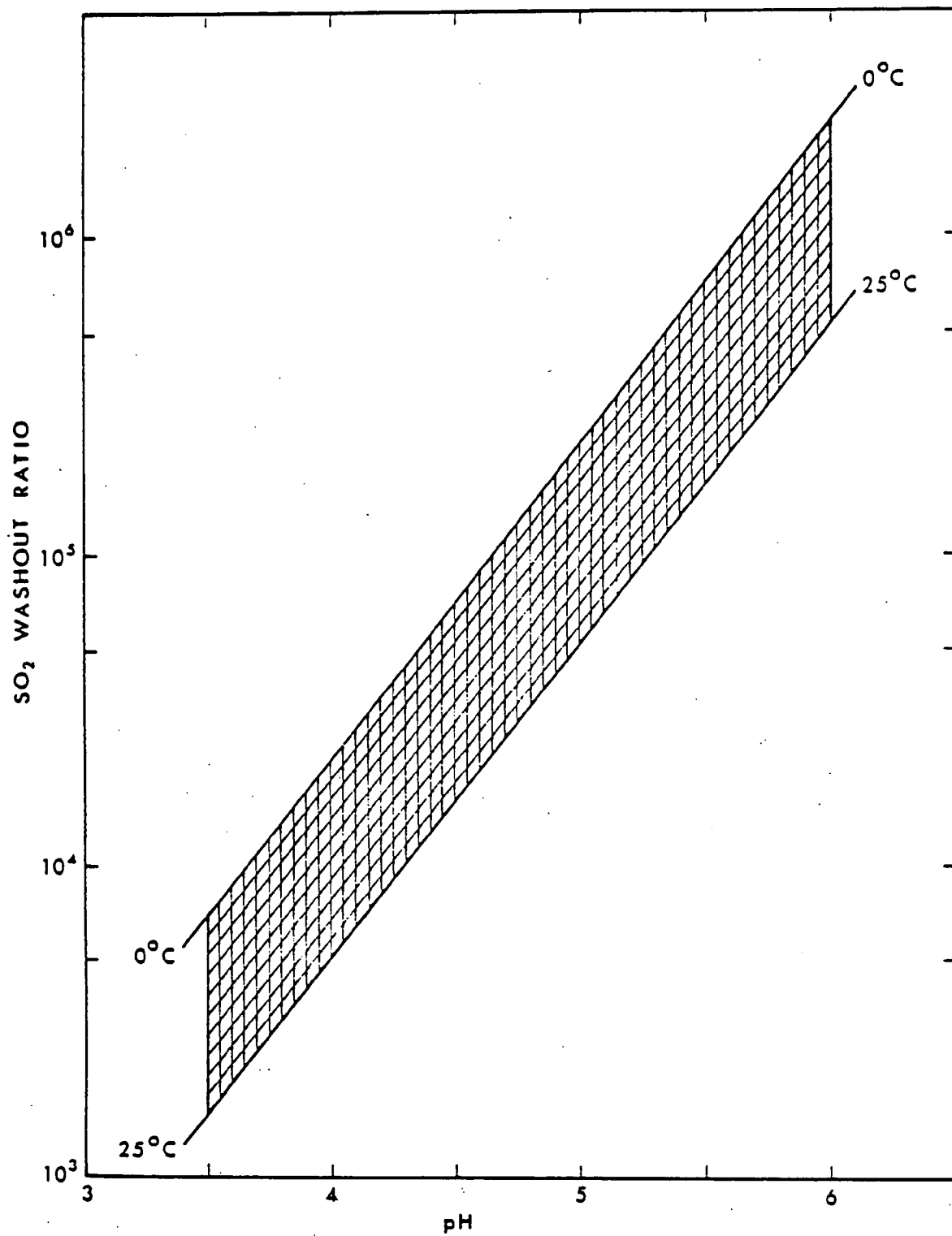


Figure 13  $\text{SO}_2$  Washout Ratio as a Function pH and Temperature for Equilibrium Scavenging Conditions  
Source: Barrie (1981)

TABLE 7. DEFAULT VALUES OF THE SCAVENGING COEFFICIENT, ( $s^{-1}$ )

<u>Pollutant</u>	<u>Liquid Precipitation</u>	<u>Frozen Precipitation</u>
SO <sub>2</sub>	$3 \times 10^{-5}$	0.0
SO <sub>4</sub> <sup>=</sup>	$1 \times 10^{-4}$	$3 \times 10^{-5}$
NO <sub>x</sub>	0.0	0.0
HNO <sub>3</sub>	$6 \times 10^{-5}$	0.0
NO <sub>3</sub> <sup>-</sup>	$1 \times 10^{-4}$	$3 \times 10^{-5}$

similar to  $\text{SO}_4^=$  is appropriate for  $\text{HNO}_3$ . Levine and Schwartz (1982) emphasize the sensitivity of  $\text{HNO}_3$  removal to the raindrop size distribution, especially to the lower radii limit of the distribution because of the dominant contribution of the smaller drops to the removal rate. Their recommendations suggest a scavenging ratio of  $6.5 \times 10^{-5} \text{ s}^{-1}$  for a rainfall rate of 1 mm/hr. Based on the low solubility of  $\text{NO}_x$ , a negligible scavenging coefficient is expected.

A precipitation code determined from the surface observations of precipitation type/intensity is used to determine if the value of  $\lambda$  for liquid or frozen precipitation is most appropriate. Precipitation observations are converted to precipitation codes as shown in Table 8. The liquid precipitation values of  $\lambda$  are used for precipitation codes 1-18; the frozen precipitation values are used for codes 19-45.

## 2.6 Puff Sampling Function

Puff superposition models such as MESOPUFF II represent a continuous plume with a number of discrete puffs. The concentration at a receptor is calculated by summing the contributions of each nearby puff, generally evaluated by taking a "snapshot" of each puff at particular time intervals (sampling steps) specified as a program input. The concentration at a receptor due to a horizontally symmetric with a Gaussian distribution is given by:

$$C(s) = \frac{Q(s)}{2\pi\sigma_y^2(s)} g(s) \exp\left[-\frac{r^2(s)}{2\sigma_y^2(s)}\right] \quad (2-58)$$

$$g(s) = \frac{2}{\sqrt{2\pi}\sigma_z} \sum_{n=-\infty}^{\infty} \exp\left[-\frac{1}{2} \frac{(H_e + 2nz_i)^2}{\sigma_z^2(s)}\right] \quad (2-59)$$

**TABLE 8. CONVERSION OF REPORTED PRECIPITATION TYPE/INTENSITY TO PRECIPITATION CODES**

**Liquid Precipitation**

<u>Precipitation Code</u>	<u>Type</u>	<u>Intensity</u>
1	Rain	Light
2	Rain	Moderate
3	Rain	Heavy
4	Rain Showers	Light
5	Rain Showers	Moderate
6	Rain Showers	Heavy
7	Freezing Rain	Light
8	Freezing Rain	Moderate
9	Freezing Rain	Heavy
10	Not Used	-
11	Not Used	-
12	Not Used	-
13	Drizzle	Light
14	Drizzle	Moderate
15	Drizzle	Heavy
16	Freezing Drizzle	Light
17	Freezing Drizzle	Moderate
18	Freezing Drizzle	Heavy

**Frozen Precipitation**

<u>Precipitation Code</u>	<u>Type</u>	<u>Intensity</u>
19	Snow	Light
20	Snow	Moderate
21	Snow	Heavy
22	Snow Pellets	Light
23	Snow Pellets	Moderate
24	Snow Pellets	Heavy
25	Not Used	-
26	Ice Crystals	*
27	Not Used	-
28	Snow Showers	Light
29	Snow Showers	Moderate
30	Snow Showers	Heavy
31	Not Used	-
32	Not Used	-
33	Not Used	-
34	Snow Grains	Light
35	Snow Grains	Moderate
36	Snow Grains	Heavy
37	Ice Pellets	Light
38	Ice Pellets	Moderate
39	Ice Pellets	Heavy
40	Not Used	-
41	Hail	*
42	Not Used	-
43	Not Used	-
44	Small Hail	*
45	Not Used	-

---

\* Intensity not currently reported for ice crystals, hail and small hail.

where,  $C(s)$  is the ground-level concentration,  
 $s$  is the distance travelled by the puff,  
 $Q(s)$  is the mass of pollutant in the puff,  
 $\sigma_y(s)$  is the standard deviation of the Gaussian distribution  
in the horizontal,  
 $\sigma_z(s)$  is the standard deviation of the Gaussian distribution  
in the vertical,  
 $r(s)$  is the radial distance from the puff center,  
 $z_i$  is the mixed-layer height, and  
 $H_e$  is the effective height of the puff center.

The vertical term,  $g(s)$  reduces to the uniformly mixed limit of  $1/z_i$  for  $\sigma_z/z_i \geq 1.6$ . In general, puffs within the daytime mixed layer satisfy this criterion about an hour or two after release.

With Equation 2-58, an accurate representation of the continuous plume depends upon the puff release rate and sampling rate being sufficient to ensure that adjacent puffs overlap. Ludwig et al. (1977) have shown that if puff separation distances exceed  $\sim 2\sigma_y$ , inaccurate results may be obtained. The frequent sampling and/or puff release necessary to satisfy the  $2\sigma_y$  criterion in the near-field of a source (where it is most restrictive) has a negative impact on model storage and computational requirements. Ludwig et al. (1977) recommend uniform space rather than uniform time release of puffs with a puff merging scheme to reduce the total number of puffs on the grid. However, frequent sampling or puff release is still necessary for near-field receptors. An alternate approach suggested by R. Yamartino (personal communication) and used in MESOPUFF II is to integrate Equation 2-58 over the distance of puff travel,  $\Delta s$ , during one sampling step.

$$\bar{C} = \frac{1}{\Delta s} \int_s^{s + \Delta s} \frac{Q(s) g(s)}{2\pi \sigma_y^2(s)} \exp \left[ \frac{-r^2(s)}{2\sigma_y^2(s)} \right] ds \quad (2-60)$$

If it is assumed that the most significant  $s$  dependence during the sampling step is in the  $r(s)$  and  $Q(s)$  terms, this integral can be evaluated. Assuming the trajectory segment is a straight line and transforming  $s$  to a dimensionless trajectory variable,  $p$ , results in:

$$r^2(p) = (X_t - X_r + p\Delta X)^2 + (Y_t - Y_r + p\Delta Y)^2 \quad (2-61)$$

where  $p = 0, 1$  correspond to the beginning and end points of the trajectory  $(X_t, Y_t)$  and  $(X_{t+1}, Y_{t+1})$ , respectively,  $(X_r, Y_r)$  are the receptor coordinates, and  $\Delta X, \Delta Y$  are the incremental  $X$  and  $Y$  distances travelled by the puff during the sampling step.

Equation 2-60 becomes:

$$\bar{C} = \frac{g}{2\pi\sigma_y^2} \int_0^1 Q(p) \exp \left[ -\frac{r^2(p)}{2\sigma_y^2} \right] dp \quad (2-62)$$

The exponential variation of  $Q$  due to removal and chemical transformation processes is expressed as a linear function over the sampling interval:

$$Q(p) = Q_t + p(Q_{t+1} - Q_t) \quad (2-63)$$

Substituting Equation 2-63 into 2-62 results in:

$$\bar{C} = \frac{g}{2\pi\sigma_y^2} Q_t \int_0^1 \exp \left[ -\frac{r^2(p)}{2\sigma_y^2} \right] dp +$$

$$(Q_{t+1} - Q_t) \int_0^1 p \exp \left[ -\frac{r^2(p)}{2\sigma_y^2} \right] dp \quad (2-64)$$

The integrals in Equation 2-64 can be solved analytically and expressed in terms of error functions and exponentials.

$$\bar{C} = \frac{g}{2\pi\sigma_y^2} \left[ Q_0 I_1 + (Q_n - Q_0) I_2 \right] \quad (2-65)$$

$$I_1 = \sqrt{\frac{\pi}{2a}} \exp \left[ 1/2 (b^2/a - c) \right] \left\{ \operatorname{erf} \left[ \frac{a+b}{\sqrt{2a}} \right] - \operatorname{erf} \left[ \frac{b}{\sqrt{2a}} \right] \right\} \quad (2-66)$$

$$I_2 = -\frac{b}{a} I_1 + \frac{1}{a} \exp \left[ 1/2 (b^2/a - c) \right] \left\{ \exp \left[ -\frac{1}{2} b^2/a \right] - \exp \left[ -\frac{1}{2} (a+2b+b^2/a) \right] \right\} \quad (2-67)$$

$$a = (\Delta x^2 + \Delta y^2) / \sigma_y^2 \quad (2-68)$$

$$b = [\Delta x(x_{t+1} - x_r) + \Delta y(y_{t+1} - y_r)] / \sigma_y^2 \quad (2-69)$$

$$c = [(x_{t+1} - x_r)^2 + (y_{t+1} - y_r)^2] / \sigma_y^2 \quad (2-70)$$

The vertical term,  $g$ , and  $\sigma_y$  are evaluated at the midpoint of the trajectory ( $p=0.5$ ).

Because the integrated contribution of each puff over the sampling step is computed, this sampling function eliminates the problem of insufficient puff overlap. Table 9 contains the results of sampling tests performed with the conventional sampling algorithm (e.g., as in MESOPUFF) and the new sampling function used in MESOPUFF II. The analytic (straight-line) Gaussian solution is also shown. As expected, the conventional algorithm produces inaccurate results when the puff separation exceeds  $2\sigma_y$ . The puff separation is  $u\delta t$ , where  $u$  is the wind speed (5 m/s),  $\delta t$  is the

TABLE 9. EFFECT OF SAMPLING RATE, N, ON PREDICTED NEAR-FIELD ( $\leq 50$  km) CONCENTRATIONS FOR TWO SAMPLING ALGORITHMS. PRESENTED ARE VALUES OF  $C/Q \times 10^7$ . N IS IN SAMPLES PER HOUR.  
(Wind Speed - 5.0 m/s, PGT Stability D, Mixing Height = 1,000 m, Uniform Vertical Distribution)

<u>Distance</u> <u>(km)</u>	$\sigma_y$ <u>(m)</u>	<u>Straight Line</u> <u>Gaussian Eqn.</u>	<u>Conventional Sampling Algorithm</u>					<u>MESOPUFF II Sampling Algorithm</u>				
			<u>N=1</u>	<u>N=2</u>	<u>N=4</u>	<u>N=8</u>	<u>N=16</u>	<u>N=1</u>	<u>N=2</u>	<u>N=4</u>	<u>N=8</u>	<u>N=16</u>
10	518	1.54	0.00	1.32	0.69	0.57	1.50	1.69	1.09	1.33	1.51	1.55
20	966	0.83	0.54	0.28	0.23	0.82	0.80	0.59	0.72	0.81	0.83	0.83
30	1,392	0.57	0.00	0.11	0.45	0.56	0.56	0.63	0.54	0.59	0.57	0.57
40	1,803	0.44	0.11	0.09	0.45	0.43	0.43	0.39	0.44	0.45	0.44	0.44
50	2,203	0.36	0.25	0.16	0.36	0.35	0.35	0.41	0.37	0.36	0.36	0.36

sampling interval ( $\delta t = 3600s/N$ ), and  $N$  is the sampling rate (samples per hour). The  $2\sigma_y$  criterion is not satisfied for  $N=1$  or  $2$  even at  $50$  km, resulting in 'gaps' in the concentration distribution. More accurate results are obtained with the MESOPUFF II algorithm. Acceptable results (i.e., within  $\sim 5\%$ ) are obtained beyond  $20$  km with  $N=2$  vs.  $N=8$  for the conventional algorithm. The major source of error in the MESOPUFF II algorithm is due to the assumption of constant  $\sigma_y$  during the sampling interval. The value of  $\sigma_y$  is evaluated at the midpoint of the trajectory segment. Thus, during the first half of the trajectory  $\sigma_y$  is somewhat overestimated; during the second half,  $\sigma_y$  is underestimated. Because the length of each trajectory segment is proportional to the wind speed, this error may be minimized by increasing the sampling rate at higher wind speeds. MESOPUFF II offers the option to dynamically determine the sampling for each puff as follows:

$$N = 1 + \frac{u}{u_c} \quad (2-71)$$

where  $u_c$  is a reference wind speed specified by the user. For example, for a  $u_c$  of  $2$  m/s,  $N$  will be assigned values of  $1$ ,  $2$ , or  $3$  for values of  $u$  of  $1.0$ ,  $2.0$ , and  $4.0$ , respectively. The value of  $N$  given by Equation 2-71 is then compared to a user-specified minimum sampling rate; if lower,  $N$  is set equal to the minimum rate.

### SECTION 3

#### DEMONSTRATION RUN

The MESOPUFF II model has been run for a two-day test period to allow a preliminary evaluation of the  $\text{SO}_2 \rightarrow \text{SO}_4^=$  transformation mechanism and to qualitatively demonstrate the behavior of several other model algorithms. The modeled period was during the Tennessee Plume Study (TPS) which was conducted in August 1978 in the vicinity of the Cumberland Steam Plant in northwestern Tennessee (Schiermeier et al. 1979). The TPS is part of a larger EPA field program, called the Sulfur Transport and Transformation in the Environment (STATE) program, which was designed to examine the effects of  $\text{SO}_x$  emissions on regional scale sulfate concentrations.

Detailed measurements from aircraft traversing the Cumberland plume provided data on chemical processes and dispersion. Plumes from other TVA plants were also sampled when they were transported near the Cumberland plume. Plume trajectories were determined with aircraft and ground-level measurements of an injected tracer gas ( $\text{SF}_6$ ), and by tracking tetroons and a manned LAMP balloon. Four specific scenarios were studied: (1) vertical mixing during highly convective conditions to downwind distances of 50 km; (2) horizontal plume spread during stable conditions with significant wind shear to downwind distances of 300-500 km; (3) dispersion during stable conditions to distances of 400 km; and (4) dispersion and chemical changes over a diurnal cycle, with fumigation in the morning and layering in the evening. The two-day study period (August 22-23) chosen for the test run falls under Scenario 4.

The model runs were made with a 24 x 30 grid covering the area encompassed by latitudes 35°-39° N and longitudes 86°-90° W (approximately from Memphis, Tennessee in the southwest corner of the grid to southern

Indiana in the northeast part of the grid). A grid spacing of 15 km was used. Only  $\text{SO}_x$  emissions from the Cumberland Steam Plant were modeled. Meteorological data from nine surface stations and three rawinsonde stations were processed (Figure 14). Special meteorological observations available during the TPS which would not be available for an operational application of the model (e.g., soundings made at 6-hour intervals) were not used. Mixed layer averaged winds were used to advect puffs within the mixed layer. Puffs above  $z_i$  were advected with vertically averaged winds through the layer from  $z_i$  to 700 mb. The surface depletion (3-layer) dry deposition model was used. Table 10 summarizes the model run parameters.

The time history of a particular puff through a diurnal cycle is presented in Table 11. The puff was released at 0100 CST on August 23 from the Cumberland stack. The puff quickly rose well above the shallow nocturnal boundary layer to a height of about 850 m. The rapid growth of the convective boundary layer and eventual fumigation of the puff is shown in Figure 15. Following the period of relatively slow puff growth, the puff quickly becomes uniformly mixed in the vertical after entrainment into the mixed layer. The puff growth rate while above the mixed layer is given by the E stability Turner dispersion curves.

Observed and predicted mixing heights in the vicinity of the Cumberland stack are presented in Figure 16. The model appears to correctly predict the growth of the morning convective mixed layer, although afternoon mixing heights are overpredicted. However, general conclusions regarding the quantitative performance of the mixing height algorithm should not be drawn from two case studies.

Modeling of dry deposition begins when the puff is fumigated into the mixed layer for the first time (1000-1100). Dry deposition and chemical transformation are of about equal importance as depletion mechanisms for  $\text{SO}_2$  (loss rates of 1.5 - 2.5% per hour during daytime). The significance of boundary layer mixing as a limit to the deposition of pollutants is seen in the ratio  $v'_d/v_d$ . During the day when buoyancy-induced turbulence causes vigorous mixing,  $v'_d/v_d$  is nearly unity. However, during stable

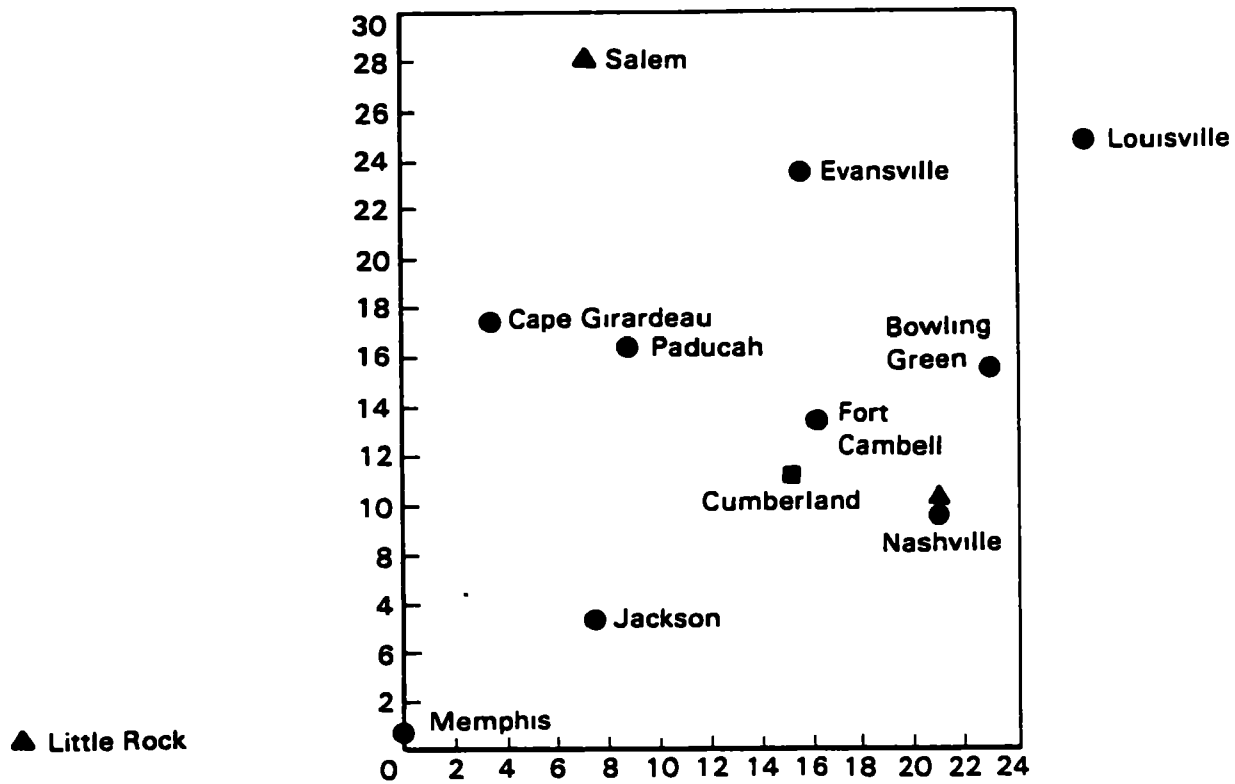


Figure 14 Location of Cumberland Steam Plant (■), Surface Meteorological Stations (●) and Upper Air Rawinsonde Stations (▲) on Meteorological Grid

TABLE 10. MODEL RUN PARAMETERS USED IN DEMONSTRATION RUN

Pollutants	SO <sub>2</sub> , SO <sub>4</sub> <sup>=</sup>
Grid Size	24 x 30
Grid spacing	15 km
Time step	1 Hour
Sampling Rate	Variable - $u_c = 2.0$ m/s (see Equation 2-71) minimum rate = 4 (Aug. 22), 2 (Aug. 23)
Puff Release Rate	1 puff/hour
Background Ozone	
Concentration	80 ppb
Puff Growth Rate above	
Boundary Layer	E stability

TABLE 11. HISTORY OF PUFF RELEASED 8/23/78 HOUR 1

Hour (CST)	$x_t$ (km)	$\sigma_y$ (m)	$\sigma_z$ (m)	$z_i$ (m)	$z_i$ (MAX) (m)	Puff <sup>(i)</sup> Code	$K_1$ (ii) (%/hr)	$v_d$ (cm/s)	$\frac{v_d}{v_d}$	$K_d$ (iii) (%/hr)	$\frac{Q_m}{Q_t}$
1	0	1	1	-	-	3	-	-	-	-	0.
2	7	278	55	11	-	3	0.2	-	-	-	0.
3	17	603	82	29	-	3	0.2	-	-	-	0.
4	26	915	102	11	-	3	0.2	-	-	-	0.
5	37	1226	118	11	-	3	0.2	-	-	-	0.
6	47	1543	134	17	-	3	0.2	-	-	-	0.
7	58	1862	147	124	-	3	2.0	-	-	-	0.
8	69	2164	159	298	-	3	2.4	-	-	-	0.
9	79	2444	170	551	-	3	1.9	-	-	-	0.
10	88	2712	179	782	-	3	1.4	-	-	-	0.
11	99	3577	1703	955	955	1	2.4	0.82	1.00	2.9	1.0
12	117	5527	*	1120	1120	2	2.4	0.81	0.96	2.4	1.0
13	135	7326	*	1311	1311	2	2.2	0.83	0.96	2.3	1.0
14	155	9127	*	1417	1417	2	2.1	0.83	0.96	2.1	1.0
15	180	11002	*	1485	1485	2	2.0	0.85	0.96	2.0	1.0
16	201	12801	*	1510	1510	2	1.8	0.75	0.96	1.6	1.0
17	219	14527	*	1519	1519	2	1.0	0.83	0.95	1.8	1.0
18	235	16327	*	1497	1519	2	0.9	0.80	0.94	1.8	0.99
19	248	18127	*	1389	1519	2	0.6	0.28	0.47	0.3	0.91
20	259	19777	*	54	1519	6	0.2	0.28	0.26	0.1	0.03

\*Puff Uniformly Mixed in Vertical -  $\sigma_z$  not calculated

(i) Puff codes: 1 = puff within mixed layer and Gaussian  
 2 = puff within mixed layer and uniform  
 3 = puff above mixed layer and Gaussian  
 6 = puff currently above (but previously below) mixed layer and uniform

(ii)  $K_1$  =  $SO_2 \rightarrow SO_4^-$  transformation rate

(iii)  $K_d$  =  $SO_2$  dry deposition depletion rate

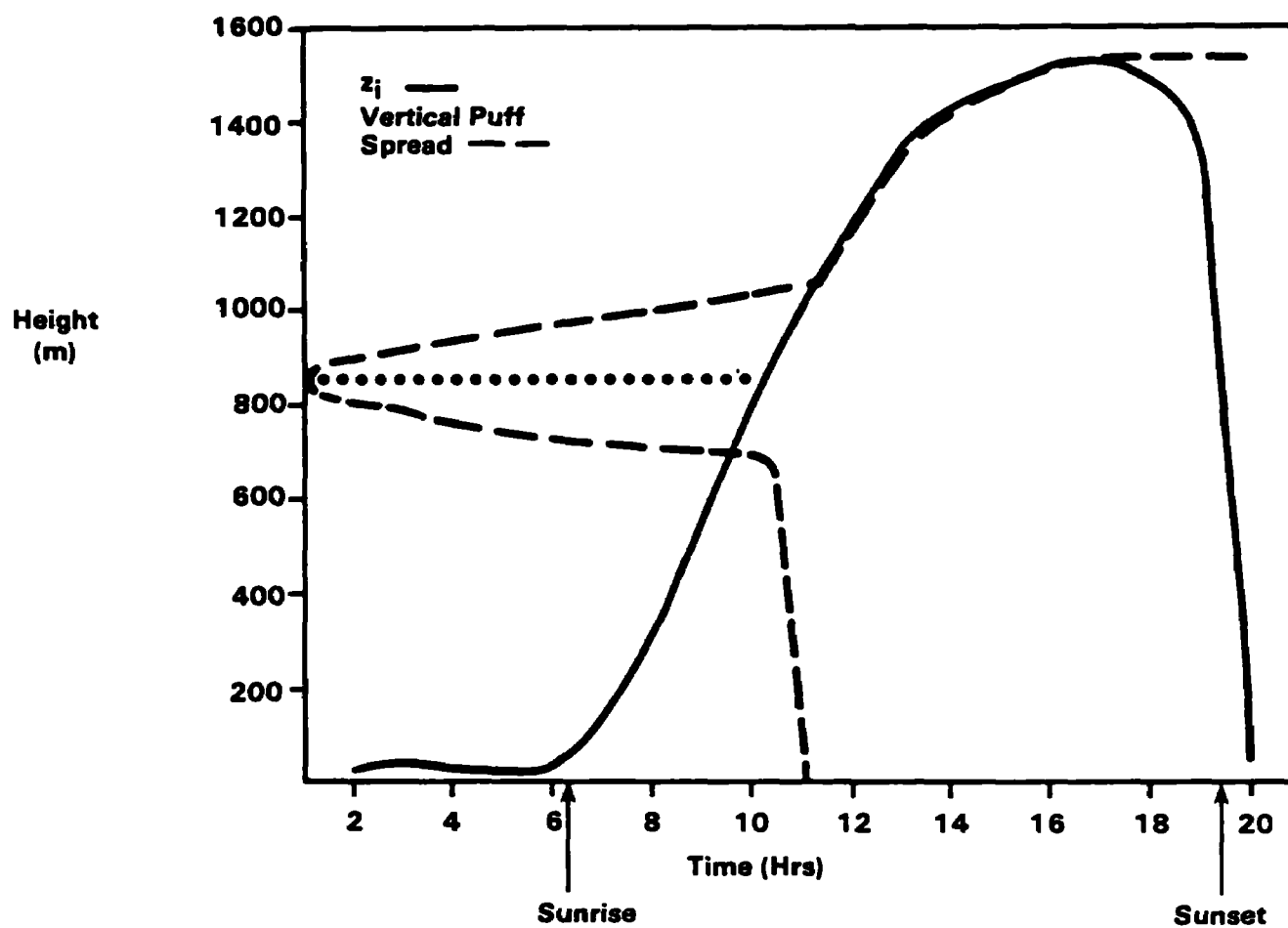


Figure 15 Boundary Layer Growth and Plume Fumigation

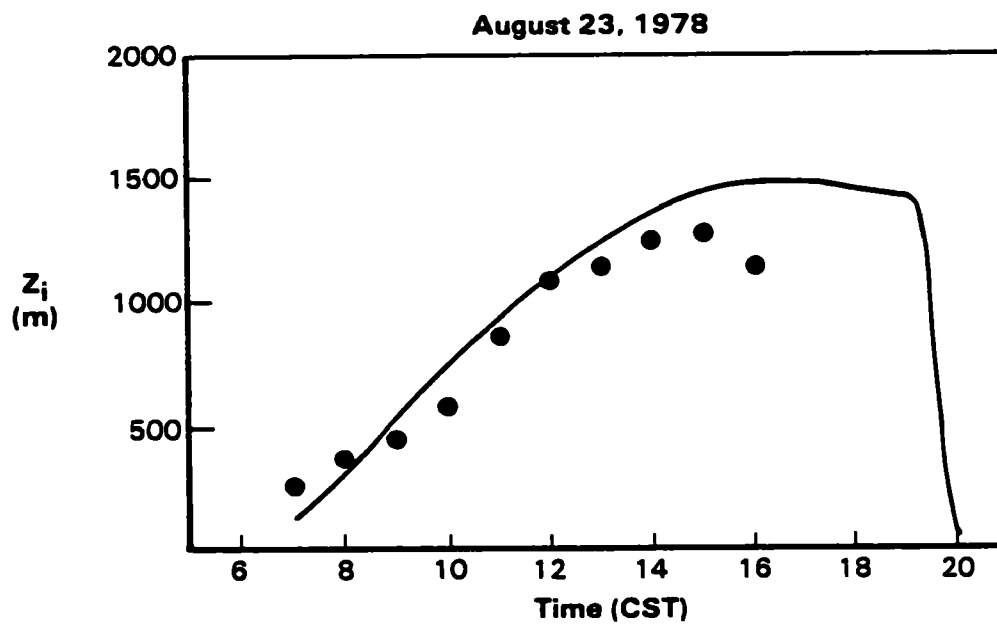
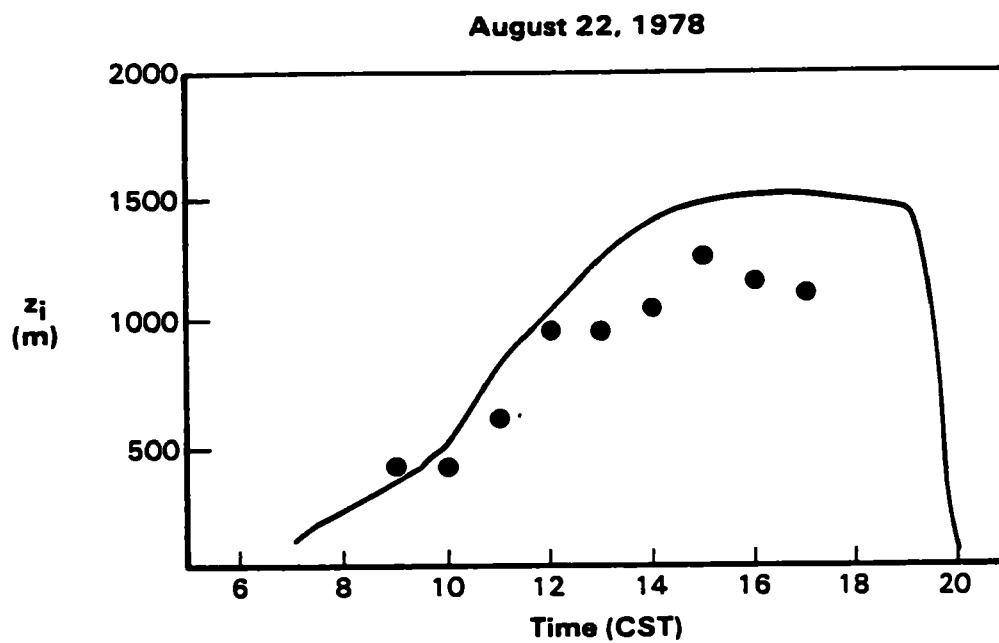


Figure 16 Observed (●) and Predicted (—) Mixing Heights in the Vicinity of the Cumberland Steam Plant

nighttime conditions,  $v'_d/v_d \ll 1$ , indicating the importance of the boundary layer mixing rate as an additional resistance to mass transfer. At 2000, the surface concentration ( $C_s$ ) is only about 1/4 of the layer-averaged concentration ( $C_m$ ). This lower near-surface concentration reduces dry deposition flux, thus increasing the lifetime of  $SO_2$  in the atmosphere.

Predicted  $SO_2$  to  $SO_4^=$  conversion rates have been calculated and compared to observations reported by Gillani et al. (1981). The average conversion rate between the time of puff release and sampling is given by Gillani et al. (1981) as:

$$k_1 = \frac{C}{\Delta t} \frac{Q_{SO4}}{Q_t} \quad (3-1)$$

$$C_f = \frac{2}{1 + Q_{SO2}/Q_t} [1 - 0.5 \ln (Q_o/Q_t)] \quad (3-2)$$

where

- $k_1$  is the average  $SO_2$  to  $SO_4^=$  conversion rate,
- $C_f$  is a correction factor accounting for changes in puff mass during the period of travel,
- $Q_o$  is the total initial sulfur mass in the puff ( $SO_2 + SO_4^=$ ) weighted as  $SO_2$ ,
- $Q_T$  is the total sulfur mass in the puff at the sampling time,
- $Q_{SO2}$  is the mass of  $SO_2$  in the puff at the sampling time,
- and,
- $Q_{SO4}$  is the mass of  $SO_4$  in the puff at the sampling time.

The MESOPUFF II conversion rates as well as those predicted by Gillani et al. (1981) are shown with observed rates in Table 12. Both schemes predict rates generally within the range of observed transformation rates during August 22. This day was generally sunny and relatively dry (low relative humidity).  $SO_2$  oxidation was probably dominated by gas phase reactions. During August 23, however, a maritime tropical air mass characterized by high humidity and hazy conditions existed in the region.

TABLE 12. OBSERVED AND PREDICTED SO<sub>2</sub> CONVERSION RATES

<u>DATE</u>	<u>Transport Time Obs. Plume (CST)</u>	<u>Plume Age (Hours)</u>	<u>Observed Rate (%/hour)</u>	<u>Predicted Rate (Gillani et al. 1981) (%/hour)</u>	<u>Transport Time Pred. Plume* (CST)</u>	<u>Plume Age (Hours)</u>	<u>Predicted Rate Eq. 2-49 and Eq. 2-52</u>
8/22	2:55 - 6:25 2:50 - 6:50	3.5-4.0	0.1 - 0.45	0.05	3:00 - 6:45	3.75	0.59
	11:30 - 13:30	2.0	1.2 - 1.7	1.4 - 1.7	11:00 - 13:00	2.0	1.5
	11:00 - 14:30	3.5	1.5 - 1.8	1.9 - 2.0	11:00 - 14:30	3.5	1.7
8/23	6:30 - 10:30	4.0	1.7 - 2.8	0.3	6:00 - 10:00	4.0	2.0
	6:00 - 11:25	5.4	2.1 - 2.5	0.4	6:00 - 11:30	5.5	2.1
	5:15 - 15:15	10.0	2.7 - 2.9	0.9 - 1.0	5:00 - 15:00	10.0	1.9
	6:15 - 16:15	10.0	2.4 - 3.3	1.0 - 1.1	6:00 - 16:00	10.0	2.0

\*Puffs released at hourly intervals

Low clouds increased during the day and dissipated after sunset. Significant plume-cloud interactions were reported by Gillani et al. (1981) during the late morning and early afternoon hours. The conversion rates predicted by MESOPUFF II are within the observed range during the morning transition period. However, the conversion rates averaged through the day are underpredicted, probably due to enhanced aqueous phase reactions associated with plume-cloud interactions. The empirical aqueous phase term of the rate equations is based on surface relative humidity measurements and is not able to account for these interactions. The Gillani et al. (1981) relationship is intended for conditions when gas phase reactions dominate (i.e., relative humidity < 75%). Therefore, it cannot account for the high observed rates during August 23 when liquid phase reactions contribute significantly.

In summary, MESOPUFF II modeling results for a limited two-day period during the TPS have been presented. The qualitative behavior of several model algorithms, including plume growth, development of the convective boundary layer, plume fumigation, and deposition processes have been presented. In particular, an encouraging preliminary evaluation of the  $\text{SO}_2$  to  $\text{SO}_4^-$  chemical transformation algorithm has been presented. These results represent only a brief and limited evaluation. Further evaluation with TPS data and additional regional-scale monitoring/experimental measurement studies are recommended.

## REFERENCES

- Atkinson, R. and A.C. Lloyd 1980. "Evaluation of Kinetic and Mechanistic Data for Photochemical Smog Chamber Modeling", EPA Contract No. 68-02-3280, ERT Document No. P-A040.
- Atkinson, R., A.C. Lloyd, L. Wings 1982. An Updated Chemical Mechanism for Hydrocarbon/ $\text{NO}_x$ / $\text{SO}_x$  Photooxidations Suitable for Inclusion in Atmospheric Simulation Models, Atmos. Environ., 16, 1341.
- Barrie, L.A. 1981. The Prediction of Rain Acidity and  $\text{SO}_2$  Scavenging in Eastern North America. Atmos. Environ., 15, 31-41.
- Benkley, C.W. and A. Bass 1979a. User's Guide to MESOPLUME Mesoscale Plume Segment Model. EPA 600/7-79-xxx, U.S. Environmental Protection Agency, Research Triangle Park, NC. 141 pp.
- Benkley, C.W. and A. Bass 1979b. User's Guide to MESOPUFF (Mesoscale Puff Model). EPA 600/7-79-xxx, U.S. Environmental Protection Agency, Research Triangle Park, NC. 124 pp.
- Benkley, C.W. and A. Bass 1979c. User's Guide to MESOPAC Mesoscale Meteorology Package. EPA 600/7-79-xxx. U.S. Environmental Protection Agency, Research Triangle Park, NC. 76 pp.
- Briggs, G.A. 1975. Plume Rise Predictions. Lectures on Air Pollution and Environmental Impact Analyses. American Meteorological Society, Boston, MA, pp 59-111.
- Brost, R.A. and J.C. Wyngaard 1978. A Model Study of the Stably Stratified Planetary Boundary Layer. J. Atmos. Sci. 35, 1427-1400.
- Calvert, J.G., F. Su, J.W. Bottenheim and O.P. Strausz 1978. Mechanism of the Homogeneous Oxidation of Sulfur Dioxide in the Troposphere. Atmos. Environ., 12, 197.
- Chamberlain, A.C. and R.C. Chadwick 1953. Deposition of Airborne Radio-Iodine Vapor. Nucleonics, 8, 22-25.
- Deardorff, J.W. and Willis, G.E. 1975. A parameterization of diffusion into the mixed layer. J. Appl. Meteor., 14:1451-1458.
- Draxler, R.R. 1977. A Mesoscale Transport and Diffusion Model. National Oceanic and Atmospheric Administration Tech. Memo. ERL-ARL-64, Air Resources Laboratories, Silver Springs, MD.
- Draxler, R.R. 1979. Modeling the Results of Two Recent Mesoscale Dispersion Experiments. Atmos. Environ. 13, 1523-1533.

- Fisher, B.E.A. 1980. Long-range Transport and Deposition of Sulfur Oxides. CERL internal report, Central Electricity Research Laboratories, Leatherhead, Surrey, United Kingdom.
- Forrest, J., R.W. Garber and L. Newman 1981. Conversion Rates in Power Plant Plumes Based on Filter Pack Data: The Coal-fired Cumberland Plume. Atmos. Environ., 15, 2273.
- Garland, J.A. 1978. Dry and wet removal of sulfur from the atmosphere. Atmos. Environ., 12, 349-362.
- Gifford, F.A. 1981. Horizontal Diffusion in the Atmosphere: A Lagrangian-Dynamical Theory. LA-8667-MS, Los Alamos Scient. Lab., P.O. Box 1663, Los Alamos, NM, 87545, 19 pp.
- Gillani, N.V., S. Kohli and W.E. Wilson 1981. Gas-to-Particle Conversion of Sulfur in Power Plant Plumes: I. Parameterization of the Gas Phase Conversion Rates for Dry, Moderately Polluted Ambient Conditions. Atmos. Environ., 15, 2293-2313.
- Hefter, J.L. 1965. The Variations of Horizontal Diffusion Parameters with Time for Travel Periods of One Hour or Longer. J. Appl. Meteor., 4, 153-156.
- Hegg, D.A. and P.V. Hobbs 1981. Cloud Water Chemistry and the Production of Sulfate in Clouds. Atmos. Environ., 15, 1597-1604.
- Henry, R.C., D.A. Godden, G.M. Hidy, and N.J. Lordi 1980. Simulation of Sulfur Oxide Behavior in Urban Areas. ERT Document P-A070-200. Prepared for the American Petroleum Institute.
- Henry, R.C. and G.M. Hidy 1981. Discussion of Multivariate Analysis of Particulate Sulfate and Other Air Quality Variables, Part I. Annual data from Los Angeles and New York. Atmos. Environ., 15, 424.
- Henry, R.C. and G.M. Hidy 1982. Multivariate Analysis of Particulate Sulfate and Other Air Quality Variables by Principle Components - II. Salt Lake City, Utah and St. Louis, Missouri. Atmos. Environ., 16, 929-943.
- Hicks, B.B. and J.D. Shannon 1979. A method for modeling the deposition of sulfur by precipitation over regional scales. J. Appl. Meteor., 18, 1415-1420.
- Hicks, B.B. 1982. Critical Assessment Document on Acid Deposition, Chapter VII - Dry Deposition. ATDL contribution file no. 81/24.
- Horst, T.W. 1977. A Surface Depletion Model for Deposition from a Gaussian Plume. Atmos. Environ., 11, 41-46.

- Levine, S.Z. and S.E. Schwartz 1982. In-Cloud and Below-Cloud of Scavenging of Nitric Acid Vapor. Atmos. Environ., 16, 1725-1734.
- Ludwig, F.L., L.S. Gasidrek, and R.E. Ruff 1977. Simplification of a Gaussian Puff Model for Real-Time Minicomputer Use. Atmos. Environ., 11, 431-436.
- Maahs, H.G. 1982. The Importance of Ozone in the Oxidation of Sulfur Dioxide in Nonurban Tropospheric Clouds. 2nd Symposium on the Composition of the Nonurban Troposphere, Amer. Meteorological Society, Williamsburg, VA, May 1982.
- Martin, L.R., D.E. Damschen and H.S. Judeikis 1981. The Reactions of Nitrogen Oxides with SO<sub>2</sub> in Aqueous Aerosols. Atmos. Environ. 15:191-195.
- Martin, L.R. 1982. Kinetic Studies of Sulfite Oxidation in Aqueous Solution, to be published in "SO<sub>2</sub>, NO and NO<sub>2</sub> Oxidation Mechanisms: Atmospheric Considerations, ed. J.G. Calvert, Ann Arbor Science, Woburn, MA.
- Maul, P.R. 1980. Atmospheric Transport of Sulfur Compound Pollutants. Central Electricity Generating Bureau MID/SSD/80/0026/R. Nottingham, England.
- Morris, C.S., C.W. Benkley, and A. Bass 1979. User's Guide to MESOGRID (Mesoscale Grid) Model. EPA-600/7-79-xxx. U.S. Environmental Protection Agency, Research Triangle Park, NC. 118 pp.
- Newman, L. 1981. Atmospheric Oxidation of Sulfur Dioxide: A Review as Viewed from Power Plant and Smelter Plume Studies. Atmos. Environ., 15, 2231.
- Penkett, S.A., B.M.R. Jones, K.A. Brice and A.E.J. Eggleton 1979. The Importance of Atmospheric Ozone and Hydrogen Peroxide in Oxidizing Sulfur Dioxide in Cloud and Rainwater. Atmos. Environ., 13, 123-137.
- Richards, L.W. et al., 1981. The Chemistry, Aerosol Physics, and Optical Properties of a Western Coal-Fired Power Plant Plume. Atmos. Environ., 15, 2111.
- Schwartz, S.E., 1982. Gas-Aqueous Reactions of Sulfur and Nitrogen Oxides in Liquid-Water Clouds; to be published in SO<sub>2</sub>, NO and NO<sub>2</sub> Oxidation Mechanisms: Atmospheric Conditions, ed. J.G. Calvert. Ann Arbor Science, Woburn, MA.
- Schwartz, S.E. and W.H. White 1982. Kinetics of Reactive Dissolution of Nitrogen Oxides into Aqueous Solution, in Advan. Environ. Sci. Technol., Vol. 12, S.E. Schwartz, Ed. (New York: Wiley and Sons, Inc., 1982).

- Scire, J.S., J. Beebe, C. Benkley, and A. Bass 1979. User's Guide to the MESOFIL Postprocessing Package. EPA-600/7-79-xxx, U.S. Environmental Protection Agency, Research Triangle Park, N.C. 72 pp.
- Scire J.S., F. Lurmann, A. Bass, and S. Hanna 1983. User's Guide to the MESOPUFF II Model and Related Processor Programs. U.S. Environmental Protection Agency, Research Triangle Park, NC.
- Scott, B.C. 1978. Parameterization of sulfate removal by precipitation. J. Appl. Meteorol., 17, 1375-1389.
- Scott, B.C. 1981. Sulfate Washout Ratios in Winter Storms. J. Appl. Meteor., 20, 619-625.
- Scriven, R.A. and B.E.A. Fisher 1975. The long-range transport of airborne material and its removal by deposition and washout. Atmos. Environ., 9, 49-58.
- Sehmel, G.A. 1980. Particle and Gas Dry Deposition - A review. Atmos. Environ. 14, 983-1011.
- Sheeh, C.M., M.L. Wesely, and B.B. Hicks 1979. Estimated Dry Deposition Velocities of Sulfur over the Eastern United States and Surrounding Regions. Atmos. Environ. 13 (10), 1361-1368.
- Slinn, W.G., L. Hasse, B. Hicks, A. Hogan, D. Lal, P. Liss, K. Munnich, G. Sehmel, and O. Vittori 1978. Some Aspects of the Transfer of Atmospheric Trace Constituents Past the Air-Sea Interface. Atmos. Environ., 12: 2055-2087.
- Smith, F.B. 1981. The significance of wet and dry synoptic regions on long-range transport of pollution and its deposition. Atmos. Environ., 15, 863-873.
- Stelson, A.W. and J.H. Seinfeld 1982. Relative Humidity and Temperature Dependence of the Ammonium Nitrate Dissociation Constant. Atmos. Environ., 16, 983-992.
- Stelson, A.W., M.E. Bassett and J.H. Seinfeld 1983. Thermodynamic Equilibrium Properties of Aqueous Solutions of Nitrate, Sulfate and Ammonium. Acid Precipitation, Chemistry of Particles, Fog and Rain Volume. J. Teasley ed., Ann Arbor Science, Woburn, MA (in press).
- Turner, D.B. 1964. A Diffusion Model for an Urban Area. J. Applied Meteorol., 3, 83-91.
- Turner, D.B. 1970. Workbook of Atmospheric Dispersion Estimates. U.S. Dept. of H.E.W., Public Health Service, Pub. 999-AP-26, 88 pp.
- U.S. EPA 1978. Guideline on Air Quality Models, OAQPS Guideline Series No. 1.2-080, EPA report No. EPA-450/2-78-027 (NTIS No. PB288783), 84 pp.

- Van Ulden, A.P. 1978. Simple estimates for vertical diffusion from sources near the ground. Atmos. Environ., 12, 2152-2129.
- Venkatram, A. 1980a. Estimating the Monin-Obukhov Length in the Stable Boundary Layer for Dispersion Calculations. Boundary-Layer Meteorology 19, 481-485.
- Venkatram, A. 1980b. Estimation of turbulence velocity scales in the stable and the unstable boundary layer for dispersion applications. In: Eleventh NATO-CCSM International Technical Meeting on Air Pollution Modeling and its Application 54-56.
- Venkatram, A., B.E. Ley and S.Y. Wong 1982. A statistical model to estimate long-term concentrations of pollutants associated with long-term transport. Atmos. Environ., 16, 249-257.
- Wang, I.T. and P.C. Chen 1980. Estimations of Heat and Momentum Fluxes Near the Ground. Proc. 2nd Joint Conf. on Applications of Air Poll. Meteorology, New Orleans. LA, March 24-27. pp 764-769.
- Wesely, M.L., and B.B. Hicks 1977. Some factors that Affect the Deposition Rates of Sulfur Dioxide and Similar gases on Vegetation. J. Air Poll. Control Assoc. 27, pp 1110-1116.
- Wilson, W.E. 1981. Sulfate Formation in Point Source Plumes: A Review of Recent Field Studies. Atmos. Environ., 15, 2573.
- Zak, B.D. 1981. Lagrangian Measurements of Sulfur Dioxide to Sulfate Conversion Rates. Atmos. Environ., 15, 2583.

# APPENDIX A

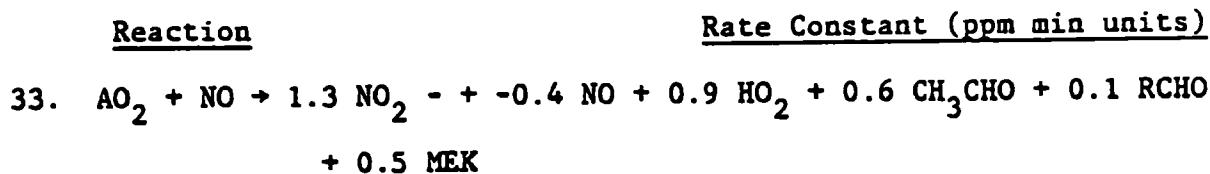
## REACTIONS AND RATE CONSTANTS OF THE ATKINSON et al. (1982) CHEMICAL MECHANISM

<u>Reaction</u>	<u>Rate Constant (ppm min units)</u>
<u>Inorganics</u>	
1. $\text{NO}_2 \rightarrow h\nu \xrightarrow{\text{O}_2} \text{NO} + \text{O}_3$	$k_1$ variable
2. $\text{NO} + \text{O}_3 \rightarrow \text{NO}_2 + \text{O}_2$	$k_2 = 1.0 \times 10^6 \text{ T}^{-1} e^{-1450/\text{T}}$
3. $\text{O}_3 + h\nu \rightarrow 2 \text{ OH}$	$k_3 = \beta_1 k_1 \times 7.6 \times 10^{-6} [\text{H}_2\text{O}]$
4. $\text{OH} + \text{NO} \xrightarrow{\text{M}} \text{HONO}$	$k_4 = 8.7 \times 10^8 \text{ T}^{-2}$
5. $\text{OH} + \text{NO}_2 \xrightarrow{\text{M}} \text{HNO}_3$	$k_5 = 1.5 \times 10^9 \text{ T}^{-2}$
6. $\text{HONO} + h\nu \rightarrow \text{OH} + \text{NO}$	$k_6 = \beta_2 k_1$
7. $\text{HO}_2 + \text{NO} \rightarrow \text{OH} + \text{NO}_2$	$k_7 = 3.7 \times 10^6 \text{ T}^{-1}$
8. $\text{HO}_2 + \text{NO}_2 \xrightarrow{\text{M}} \text{HO}_2\text{NO}_2$	$k_8 = 1.5 \times 10^8 \text{ T}^{-2}$
9. $\text{HO}_2\text{NO}_2 \xrightarrow{\text{M}} \text{HO}_2 + \text{NO}_2$	$k_9 = 7.8 \times 10^{15} e^{-10420/\text{T}}$
10. $\text{HO}_2 + \text{HO}_2 \rightarrow \text{H}_2\text{O}_2 + \text{O}_2$	$k_{10} = 3.4 \times 10^4 \text{ T}^{-1} e^{1100/\text{T}}$ $+ [\text{H}_2\text{O}] 5.8 \times 10^{-5} \text{ T}^{-2} e^{5800/\text{T}}$
11. $\text{H}_2\text{O}_2 + h\nu \rightarrow 2\text{OH}$	$k_{11} = \beta_3 k_1$
12. $\text{OH} + \text{CO} \xrightarrow{\text{O}_2} \text{HO}_2$	$k_{12} = 1.3 \times 10^5 \text{ T}^{-1}$
13. $\text{NO}_2 + \text{O}_3 \rightarrow \text{NO}_3$	$k_{13} = 5.3 \times 10^4 \text{ T}^{-1} e^{-2450/\text{T}}$
14. $\text{NO} + \text{NO}_3 \rightarrow 2\text{NO}_2$	$k_{14} = 8.4 \times 10^6 \text{ T}^{-1}$
15. $\text{NO}_2 + \text{NO}_3 \xrightarrow{\text{M}} \text{N}_2\text{O}_5$	$k_{15} = 3.1 \times 10^7 \text{ T}^{-1} e^{-1100/\text{T}}$
16. $\text{N}_2\text{O}_5 \xrightarrow{\text{M}} \text{NO}_2 + \text{NO}_3$	$k_{16} = 3.5 \times 10^{18} e^{-12280/\text{T}}$
17. $\text{N}_2\text{O}_5 + \text{H}_2\text{O} \rightarrow 2\text{HNO}_3$	$k_{17} = 6.7 \times 10^{-4} \text{ T}^{-1}$
18. $\text{NO}_3 + h\nu \rightarrow 0.3 \text{ NO} + 0.7 \text{ NO}_2$ $+ 0.7 \text{ O}_3$	$k_{18} = \beta_4 k_1$

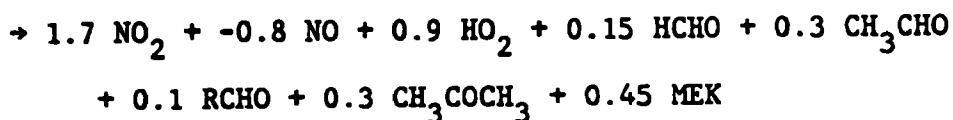
# APPENDIX A (Continued)

<u>Reaction</u>	<u>Rate Constant (ppm min units)</u>
19. $\text{OH} + \text{O}_3 \rightarrow \text{HO}_2$	$k_{19} = 7.0 \times 10^5 \text{ T}^{-1} e^{-940/T}$
20. $\text{HO}_2 + \text{O}_3 \rightarrow \text{OH}$	$k_{20} = 4.8 \times 10^3 \text{ T}^{-1} e^{-680/T}$
<u>Formaldehyde</u>	
21. $\text{HCHO} + \text{h}\nu \xrightarrow{\text{O}_2} \text{HO}_2 + \text{HO}_2 + \text{CO}$	$k_{21} = \beta_5 k_1$
22. $\text{HCHO} + \text{h}\nu \rightarrow \text{CO} + \text{H}_2$	$k_{22} = \beta_6 k_1$
23. $\text{OH} + \text{HCHO} \xrightarrow{\text{O}_2} \text{HO}_2 + \text{CO}$	$k_{23} = 4.4 \times 10^6 \text{ T}^{-1}$
<u>Acetaldehyde</u>	
24. $\text{CH}_3\text{CHO} + \text{h}\nu \xrightarrow{\text{O}_2} \text{CH}_3\text{O}_2 + \text{HO}_2 + \text{CO}$	$k_{24} = \beta_7 k_1$
25. $\text{OH} + \text{CH}_3\text{CHO} \xrightarrow{\text{O}_2} \text{CH}_3\text{CO}_3$	$k_{25} = 3.0 \times 10^6 \text{ T}^{-1} e^{250/T}$
26. $\text{CH}_3\text{CO}_3 + \text{NO}_2 \rightarrow \text{PAN}$	$k_{26} = 2.1 \times 10^6 \text{ T}^{-1}$
27. $\text{PAN} \rightarrow \text{CH}_3\text{CO}_3 + \text{NO}_2$	$k_{27} = 1.2 \times 10^{18} e^{-13543/T}$
28. $\text{CH}_3\text{CO}_3 + \text{NO} \xrightarrow{\text{O}_2} \text{NO}_2 + \text{CH}_3\text{O}_2$	$k_{28} = 3.1 \times 10^6 \text{ T}^{-1}$
29. $\text{CH}_3\text{O}_2 + \text{NO} \rightarrow \text{HCHO} + \text{HO}_2 + \text{NO}_2$	$k_{29} = 3.1 \times 10^6 \text{ T}^{-1}$
<u>Propane</u>	
30. $\text{OH} + \text{PROPANE} \rightarrow \text{PO}_2$	$k_{30} = 6.6 \times 10^6 \text{ T}^{-1} e^{-680/T}$
31. $\text{PO}_2 + \text{NO} \rightarrow \text{HO}_2 + \text{NO}_2 + \text{CH}_3\text{COCH}_3$	$k_{31} = 3.1 \times 10^6 \text{ T}^{-1}$
<u>Alkanes</u>	
32. $\text{OH} + \text{ALKANE} \rightarrow \text{AO}_2$	$k_{32} = 8.0 \times 10^6 \text{ T}^{-1} e^{-560/T}$ for explicit n-butane $k_{32} = 6.6 \times 10^6 \text{ T}^{-1} e^{-400/T}$ for lumped $\geq \text{C}_4$ alkane

# APPENDIX A (Continued)



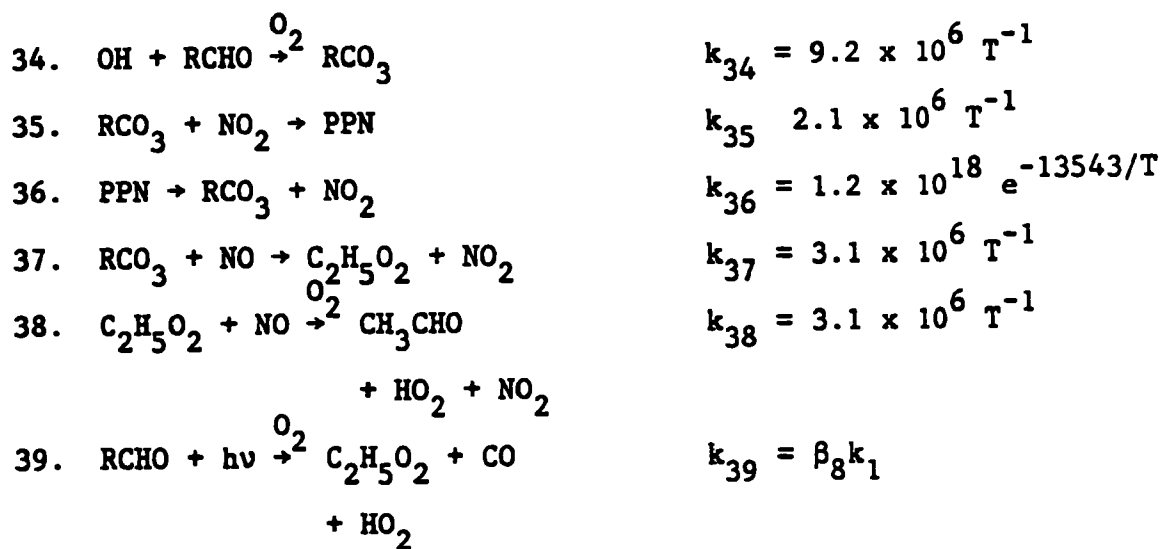
Explicit n-butane



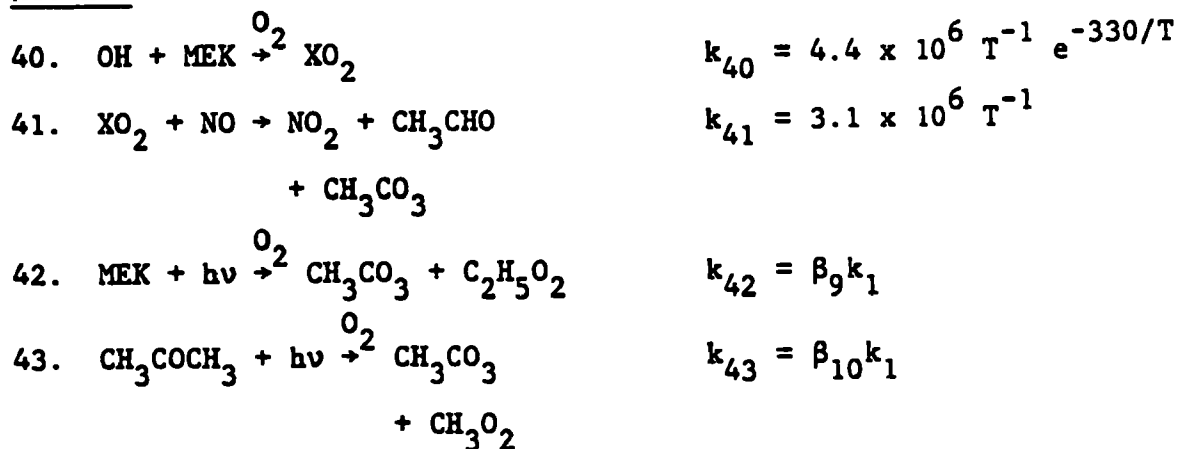
Lumped  $\geq \text{C}_4$  alkane mechanism

$$k_{33} = 3.1 \times 10^6 \text{ T}^{-1} \text{ for both systems}$$

## Higher Aldehydes



## Ketones



# APPENDIX A (Continued)

Reaction	Rate Constant (ppm min units)
<u>Alkenes</u>	
44. OH + Ethene $\xrightarrow{O_2}$ 2HCHO + HO <sub>2</sub>	$k_{44} = 9.7 \times 10^5 T^{-1} e^{380/T}$
45. OH + Propene $\xrightarrow{O_2}$ HCHO + CH <sub>3</sub> CHO + HO <sub>2</sub> + NO <sub>2</sub> - NO	$k_{45} = 1.8 \times 10^6 T^{-1} e^{540/T}$
46. OH + Butene $\xrightarrow{O_2}$ 1.8 CH <sub>3</sub> CHO + 0.9 HO <sub>2</sub> + 0.9 NO <sub>2</sub> - NO	$k_{46} = 5.0 \times 10^6 T^{-1} e^{540/T}$
47. O <sub>3</sub> + Ethene → HCHO + 0.4 $\dot{C}H_2\dot{O}_2$ + 0.4 CO + 0.12 HO <sub>2</sub>	$k_{47} = 4.2 \times 10^3 T^{-1} e^{-2560/T}$
48. O <sub>3</sub> + Propene → 0.5 HCHO + 0.5 CH <sub>3</sub> CHO + 0.2 $\dot{C}H_2\dot{O}_2$ + 0.2 CH <sub>3</sub> $\dot{C}HO\dot{O}$ + 0.3 CO + 0.2 HO <sub>2</sub> + 0.1 OH + 0.2 CH <sub>3</sub> O <sub>2</sub>	$k_{48} = 3.1 \times 10^3 T^{-1} e^{-1900/T}$
49. O <sub>3</sub> + Butenes → CH <sub>3</sub> CHO + 0.4 CH <sub>3</sub> $\dot{C}HO\dot{O}$ + 0.3 HO <sub>2</sub> + 0.2 OH + 0.45 CH <sub>3</sub> O <sub>2</sub> + 0.2 CO	$k_{49} = 3.3 \times 10^3 T^{-1} e^{-1050/T}$
50. $\dot{C}H_2\dot{O}_2$ + NO → HCHO + NO <sub>2</sub>	$k_{50} = 3.1 \times 10^6 T^{-1}$
51. $\dot{C}H_2\dot{O}_2$ + NO <sub>2</sub> → HCHO + NO <sub>2</sub>	$k_{51} = 3.1 \times 10^5 T^{-1}$
52. $\dot{C}H_2\dot{O}_2$ + SO <sub>2</sub> → HCHO + SO <sub>4</sub> <sup>=</sup>	$k_{52} = 3.0 \times 10^4 T^{-1} T^{-1}$
53. $\dot{C}H_2\dot{O}_2$ + H <sub>2</sub> O → Product	$k_{53} = 1.5 T^{-1}$
54. CH <sub>3</sub> $\dot{C}HO\dot{O}$ + NO → CH <sub>3</sub> CHO + NO <sub>2</sub>	$k_{54} = 3.1 \times 10^6 T^{-1}$
55. CH <sub>3</sub> $\dot{C}HO\dot{O}$ + NO <sub>2</sub> → CH <sub>3</sub> CHO + NO <sub>3</sub>	$k_{55} = 3.1 \times 10^5 T^{-1}$
56. CH <sub>3</sub> $\dot{C}HO\dot{O}$ + SO <sub>2</sub> → CH <sub>3</sub> CHO + SO <sub>4</sub> <sup>=</sup>	$k_{56} = 3.0 \times 10^4 T^{-1}$
57. CH <sub>3</sub> $\dot{C}HO\dot{O}$ + H <sub>2</sub> O → Product	$k_{57} = 1.5 T^{-1}$

# APPENDIX A (Continued)

<u>Reaction</u>	<u>Rate Constant (ppm min units)</u>
<u>Aromatics</u>	
58. OH + Benzene → 0.25 Cresol + 0.25 HO <sub>2</sub> + 0.75 ADD	$k_{58} = 5.3 \times 10^5 \text{ T}^{-1}$
59. OH + Toluene → 0.15 ARO <sub>2</sub> + 0.20 Cresol + 0.20 HO <sub>2</sub> + 0.65 ADD	$k_{59} = 2.7 \times 10^6 \text{ T}^{-1}$
60. OH + Xylene → 0.25 Cresol + 0.25 HO <sub>2</sub> + 0.75 ADD	$k_{60} = 7.9 \times 10^6 \text{ T}^{-1}$ for lumped xylene $= 1.05 \times 10^7 \text{ T}^{-1}$ for explicit m-xylene
61. ADD + NO → 0.75 NO <sub>2</sub> + 0.75 HO <sub>2</sub> + 0.75 DIAL + $\alpha_1$ (CHO) <sub>2</sub> + $\alpha_2$ CH <sub>3</sub> COCHO	$k_{61} = 3.1 \times 10^6 \text{ T}^{-1}$
62. OH + DIAL → E1	$k_{62} = 1.3 \times 10^7 \text{ T}^{-1}$
63. E1 + NO <sub>2</sub> → E1 NO <sub>2</sub>	$k_{63} = 2.1 \times 10^6 \text{ T}^{-1}$
64. E1 NO <sub>2</sub> → E1 + NO <sub>2</sub>	$k_{64} = 1.2 \times 10^{18} e^{-13543/T}$
65. E1 + NO → 3 NO <sub>2</sub> - 2 NO + $\alpha_3$ (CHO) <sub>2</sub> + $\alpha_4$ CH <sub>3</sub> CO <sub>3</sub> + $\alpha_4$ CH <sub>3</sub> COCHO + $\alpha_3$ CO + $\alpha_3$ HO <sub>2</sub>	$k_{65} = 3.1 \times 10^6 \text{ T}^{-1}$
66. OH + (CHO) <sub>2</sub> $\xrightarrow{O_2}$ HO <sub>2</sub> + CO	$k_{66} = 8.8 \times 10^6 \text{ T}^{-1}$
67. (CHO) <sub>2</sub> + hν → HCHO + CO	$k_{67} = \beta_{11} k_1$
68. OH + CH <sub>3</sub> COCHO $\xrightarrow{O_2}$ CH <sub>3</sub> CO <sub>3</sub> + CO	$k_{68} = 6.6 \times 10^6 \text{ T}^{-1}$
69. CH <sub>3</sub> COCHO + hν $\xrightarrow{O_2}$ CH <sub>3</sub> CO + HO <sub>2</sub> + CO	$k_{69} = \beta_{12} k_1$

# APPENDIX A (Continued)

<u>Reaction</u>	<u>Rate Constant (ppm min units)</u>
70. OH + Cresol → ADD2	$k_{70} = 1.9 \times 10^7 T^{-1}$
71. ADD2 + NO → 0.75 NO <sub>2</sub> + 0.75 HO <sub>2</sub> + 0.75 DIAL	$k_{71} = 3.1 \times 10^6 T^{-1}$
72. NO <sub>3</sub> + Cresol → HNO <sub>3</sub> + Phenoxy	$k_{72} = 6.6 \times 10^6 T^{-1}$
73. Phenoxy + NO <sub>2</sub> → Products (o-, p-nitrophenols)	$k_{73} = 6.6 \times 10^6 T^{-1}$
74. ARO <sub>2</sub> + NO → 0.75 NO <sub>2</sub> + 0.75 HO <sub>2</sub> + 0.75 ARCHO	$k_{74} = 3.1 \times 10^6 T^{-1}$
75. ARCHO + hv → Products	$k_{75} = \beta_{13} k_1$
76. OH + ARCHO $\xrightarrow{O_2}$ ARCO <sub>3</sub>	$k_{76} = 5.7 \times 10^6 T^{-1}$
77. ARCO <sub>3</sub> + NO <sub>2</sub> → PBZN	$k_{77} = 2.1 \times 10^6 T^{-1}$
78. PBZN → ARCO <sub>3</sub> + NO <sub>2</sub>	$k_{78} = 1 \times 10^{17} e^{-13025/T}$
79. ARCO <sub>3</sub> + NO → PhO <sub>2</sub> + NO <sub>2</sub>	$k_{79} = 3.1 \times 10^6 T^{-1}$
80. PhO <sub>2</sub> + NO → Phenoxy + NO <sub>2</sub>	$k_{80} = 3.1 \times 10^6 T^{-1}$
<u>SO<sub>2</sub></u>	
81. OH + SO <sub>2</sub> $\xrightarrow{M}$ SO <sub>4</sub> <sup>=</sup>	$k_{81} = 1.5 \times 10^{13} T^{-4}$

## NOTES

- 1)  $\beta_i$  = proportionality of photolytic rate for the ith photolytic reaction rate to  $k_1$ .  $\beta_i$  are a function of solar zenith angle.
- 2)  $\alpha_i$  = variable stoichiometric coefficients which depend on the benzene, toluene, and xylene concentrations.

<b>TECHNICAL REPORT DATA</b> <i>(Please read Instructions on the reverse before completing)</i>		
1. REPORT NO.	2.	3. RECIPIENT'S ACCESSION NO.
4. TITLE AND SUBTITLE DEVELOPMENT OF THE MESOPUFF II DISPERSION MODEL		5. REPORT DATE
		6. PERFORMING ORGANIZATION CODE
7. AUTHOR(S) J. S. Scire, F. W. Lurmann, A. Bass, S. R. Hanna		8. PERFORMING ORGANIZATION REPORT NO.
9. PERFORMING ORGANIZATION NAME AND ADDRESS Environmental Research & Technology, Inc. 696 Virginia Road Concord, Massachusetts 01742		10. PROGRAM ELEMENT NO. CDTA1D/02-1607 (FY-84)
		11. CONTRACT/GRANT NO. 68-02-3733
12. SPONSORING AGENCY NAME AND ADDRESS Environmental Sciences Research Laboratory--RTP, NC Office of Research and Development U.S. Environmental Protection Agency Research Triangle Park, NC 27711		13. TYPE OF REPORT AND PERIOD COVERED Final
		14. SPONSORING AGENCY CODE EPA/600/09
15. SUPPLEMENTARY NOTES		
16. ABSTRACT <p>The development of the MESOPUFF II regional-scale air quality model is described. MESOPUFF II is a Lagrangian variable-trajectory puff superposition model suitable for modeling the transport, diffusion and removal of air pollutants from multiple point and area sources at transport distances beyond the range of conventional straight-line Gaussian plume models (i.e., beyond ~ 10-50 km). It is an extensively modified version of the MESOScale PUFF (MESOPUFF) model. Major additions and enhancements include: use of hourly surface meteorological data and twice-daily rawinsonde data; separate wind fields to represent flow within and above the boundary layer; parameterization of vertical dispersion in terms of micrometeorological turbulence variables; parameterization of SO<sub>2</sub> to SO<sub>4</sub> and NO<sub>x</sub> to NO<sub>3</sub> conversion, including the chemical equilibrium of the HNO<sub>3</sub>/NH<sub>3</sub>/NH<sub>4</sub>NO<sub>3</sub> system; resistance modeling of dry deposition, including options for source or surface depletion; time- and space-varying wet removal; and a computationally efficient puff sampling function. The scientific and operational bases for these developments are described. The results of a preliminary evaluation of several model algorithms during a two-day period of the Tennessee Plume Study are also presented.</p>		
17. KEY WORDS AND DOCUMENT ANALYSIS		
a. DESCRIPTORS	b. IDENTIFIERS/OPEN ENDED TERMS	c. COSATI Field/Group
18. DISTRIBUTION STATEMENT RELEASE TO PUBLIC	19. SECURITY CLASS (This Report) UNCLASSIFIED	21. NO. OF PAGES
	20. SECURITY CLASS (This page) UNCLASSIFIED	22. PRICE

## INSTRUCTIONS

- 1. REPORT NUMBER**  
Insert the EPA report number as it appears on the cover of the publication.
- 2. LEAVE BLANK**
- 3. RECIPIENTS ACCESSION NUMBER**  
Reserved for use by each report recipient.
- 4. TITLE AND SUBTITLE**  
Title should indicate clearly and briefly the subject coverage of the report, and be displayed prominently. Set subtitle, if used, in smaller type or otherwise subordinate it to main title. When a report is prepared in more than one volume, repeat the primary title, add volume number and include subtitle for the specific title.
- 5. REPORT DATE**  
Each report shall carry a date indicating at least month and year. Indicate the basis on which it was selected (*e.g., date of issue, date of approval, date of preparation, etc.*).
- 6. PERFORMING ORGANIZATION CODE**  
Leave blank.
- 7. AUTHOR(S)**  
Give name(s) in conventional order (*John R. Doe, J. Robert Doe, etc.*). List author's affiliation if it differs from the performing organization.
- 8. PERFORMING ORGANIZATION REPORT NUMBER**  
Insert if performing organization wishes to assign this number.
- 9. PERFORMING ORGANIZATION NAME AND ADDRESS**  
Give name, street, city, state, and ZIP code. List no more than two levels of an organizational hierarchy.
- 10. PROGRAM ELEMENT NUMBER**  
Use the program element number under which the report was prepared. Subordinate numbers may be included in parentheses.
- 11. CONTRACT/GRANT NUMBER**  
Insert contract or grant number under which report was prepared.
- 12. SPONSORING AGENCY NAME AND ADDRESS**  
Include ZIP code.
- 13. TYPE OF REPORT AND PERIOD COVERED**  
Indicate interim final, etc., and if applicable, dates covered.
- 14. SPONSORING AGENCY CODE**  
Leave blank.
- 15. SUPPLEMENTARY NOTES**  
Enter information not included elsewhere but useful, such as: Prepared in cooperation with, Translation of, Presented at conference of, To be published in, Supersedes, Supplements, etc.
- 16. ABSTRACT**  
Include a brief (*200 words or less*) factual summary of the most significant information contained in the report. If the report contains a significant bibliography or literature survey, mention it here.
- 17. KEY WORDS AND DOCUMENT ANALYSIS**
  - (a) **DESCRIPTORS** - Select from the Thesaurus of Engineering and Scientific Terms the proper authorized terms that identify the major concept of the research and are sufficiently specific and precise to be used as index entries for cataloging.
  - (b) **IDENTIFIERS AND OPEN-ENDED TERMS** - Use identifiers for project names, code names, equipment designators, etc. Use open-ended terms written in descriptor form for those subjects for which no descriptor exists.
  - (c) **COSATI FIELD GROUP** - Field and group assignments are to be taken from the 1965 COSATI Subject Category List. Since the majority of documents are multidisciplinary in nature, the Primary Field/Group assignment(s) will be specific discipline, area of human endeavor, or type of physical object. The application(s) will be cross-referenced with secondary Field/Group assignments that will follow the primary posting(s).
- 18. DISTRIBUTION STATEMENT**  
Denote releasability to the public or limitation for reasons other than security for example "Release Unlimited." Cite any availability to the public, with address and price.
- 19. & 20. SECURITY CLASSIFICATION**  
DO NOT submit classified reports to the National Technical Information service.
- 21. NUMBER OF PAGES**  
Insert the total number of pages, including this one and unnumbered pages, but exclude distribution list, if any.
- 22. PRICE**  
Insert the price set by the National Technical Information Service or the Government Printing Office, if known.